Digital Comprehensive Summaries of Uppsala Dissertations from the Faculty of Pharmacy 386

Liquid crystal nanoparticles for oral antibiotic delivery

XIGUO HE

ACTA UNIVERSITATIS
UPSALIENSIS
2025

ISSN 1651-6192
ISBN 978-91-513-2620-7
urn:nbn:se:uu:diva-568292

UPPSALA
UNIVERSITET

Dissertation presented at Uppsala University to be publicly examined in A1:111a, BMC, Uppsala, Friday, 21 November 2025 at 13:15 for the degree of Doctor of Philosophy (Faculty of Pharmacy). The examination will be conducted in English. Faculty examiner: Professor Johan Engblom (Malmö universitet, Faculty of Health and Society, Department of Biomedical Sciences).

Abstract
He, X. 2025. Liquid crystal nanoparticles for oral antibiotic delivery. *Digital Comprehensive Summaries of Uppsala Dissertations from the Faculty of Pharmacy* 386. 79 pp. Uppsala: Acta Universitatis Upsaliensis. ISBN 978-91-513-2620-7.

The global rise in antimicrobial resistance has created an urgent demand for novel drug delivery strategies that can improve access to antibiotics and reduce reliance on intravenous administration. Oral therapy remains the most practical route for outpatient treatment, yet many antibiotics display poor solubility, low permeability, and instability in the gastrointestinal tract, limiting their effectiveness. Lipid-based nanocarriers, particularly liquid crystal nanoparticles (LCNPs), offer structural versatility, high internal surface area, and tunable release properties that make them attractive for enabling oral delivery.

The overall aim of this thesis was to develop LCNP-based oral formulations of clinically relevant antibiotics through an integrated approach combining molecular understanding with potential scalable manufacturing.

In the first part, antibiotic-loaded LCNPs with internal cubic and hexagonal phases were developed from non-digestible lipid building blocks and systematically evaluated for their physicochemical properties, stability in simulated intestinal fluids, and impact on representative commensal bacteria. Complementing these experimental findings, all-atom molecular dynamics simulations were employed to reveal that the studied antibiotics, clarithromycin preferentially localized within the lipid domain, whereas vancomycin resided at the lipid–water interface. Therefore, these primary results provide both experimental and molecular-level evidence for how lipid composition and nanostructure govern drug localization, stability, and release in LCNPs-based antibiotic formulations.

In the second part, the influence of internal mesophase on transepithelial permeability was investigated in intestinal models using Caco-2 cells. Compared with liposomes, non-lamellar LCNPs exhibited superior uptake via energy-independent internalization and significantly enhanced vancomycin transport across intestinal monolayers, underscoring the role of mesophase architecture in promoting oral absorption.

In the final part, a semi-solid extrusion (SSE) 3D printing platform was developed to convert vancomycin-loaded hexosomes into personalized oral tablets. LCNPs-based formulations preserved a stable hexagonal phase throughout the preparation of the printable gel, the 3D printing process, and tablet rehydration. Moreover, the printed tablets complied with European Pharmacopoeia standards for mass uniformity, drug content, and disintegration. The optimized gels displayed favorable rheological properties, ensuring precise, reproducible dosing for better patient compliance.

Keywords: antimicrobial resistance, oral delivery, liquid crystal nanoparticles, cubosomes, hexosomes, molecular dynamics, Caco-2 permeability, 3D printing, personalized antibiotic dosage form

Xiguo He, Department of Pharmacy, Box 580, Uppsala University, SE-75123 Uppsala, Sweden. Uppsala Antibiotic Center, Box 582, Uppsala University, SE-751 23 Uppsala, Sweden.

ISSN 1651-6192
ISBN 978-91-513-2620-7
URN urn:nbn:se:uu:diva-568292 (http://urn.kb.se/resolve?urn=urn:nbn:se:uu:diva-568292)

To my family, my friends and myself

“反者道之动”

老子

List of Papers

This thesis is based on the following papers, which are referred to in the text by their Roman numerals.

I. **He, X.**, Karlsson, P.A., Xiong, R., Moodie, L.W.K., Wang, H., Bergström, C.A.S., Hubert, M. (2025) Liquid crystal nanoparticles for oral combination antibiotic therapies: A strategy towards protecting commensal gut bacteria during treatment. *Journal of Colloid and Interface Science*, 678: 287–300.

II. Altun, D., **He, X.**, Bergström, C.A.S., Hubert, M., Hossain, S. (2025) Molecular dynamic simulations of a hexagonal liquid crystal phase to study drug partitioning and release mechanisms. *Colloids and Surfaces B: Biointerfaces*. (Accepted)

III. **He, X.**, Vo, D.S., Lundquist, P., Bergström, C.A.S., Hubert, M. (2025) Liquid crystal nanoparticles boost intestinal permeability of vancomycin via energy-independent uptake. *In manuscript.*

IV. **He, X.***, Kuropka, J.*, Habtemikael, L., Müller, P., Bergström, C.A.S., Hubert, M. (2025) 3D printing of liquid crystal nanoparticle containing tablets for personalized oral antibiotic delivery. *In manuscript.*

*Shared first author

Reprints were made with permission from the respective publishers.

Contents

Abbreviations

AMR	Antimicrobial resistance
API	Active pharmaceutical ingredient
ATCC	American Type Culture Collection
BMD	Broth microdilution
CFU	Colony-forming unit
CLA	Clarithromycin
CME	Clathrin-mediated endocytosis
CPP	Critical packing parameter
Cryo-TEM	Cryogenic transmission electron microscopy
Cyto D	Cytochalasin D
DLS	Dynamic light scattering
DOPC	1,2-dioleoyl-sn-glycero-3-phosphocholine
DOSY	Diffusion ordered spectroscopy
EE	Encapsulation efficacy
EUCAST	European Committee on Antimicrobial Susceptibility Testing
FAs	Fatty acids
FAR	Farnesol
G’	Storage modulus
G’’	Loss modulus
GIT	Gastrointestinal tract
GMO	Glyceryl Monooleate
GMP	Good manufacturing practice
H_{II}	Inverse hexagonal
HPLC	High-performance liquid chromatography
$L\alpha$	Lamellar
LC	Liquid crystal
LCNP	Liquid crystal nanoparticle
LVE	Linear viscoelastic
MC	Methyl cellulose
MD	Molecular dynamics
MHA	Mueller-Hinton Agar
MHB	Mueller-Hinton Broth
MIC	Minimum Inhibitory Concentration

MWCO	Molecular weight cut-off
NMR	Nuclear magnetic resonance
OVA	Ovalbumin
Papp	Apparent permeability coefficient
PDI	Polydispersity index
PEO	Polyethylene oxide
Ph. Eur.	Pharmacopoeia Europaea
PHY	Phytantriol
PHY/FAR	Phytantriol/farnesol (9:1 ratio)
PHY/TOC	Phytantriol/α-tocopherol (8:2 ratio)
PMF	Potential of mean force
PPO	Polypropylene oxide
Q_{II}	Inverse bicontinuous cubic phases
SAXS	Small-angle X-ray scattering
SSE	Semi-solid extrusion
TOC	α-tocopherol
UPLC	Ultra Performance Liquid Chromatography
US	Umbrella sampling
UV	Ultraviolet
VAN	Vancomycin
WHAM	Weighted histogram analysis method
WHO	World Health Organization
ZP	Zeta potential

Introduction

"Mr. X. has a sore throat. He buys some penicillin and gives himself, not enough to kill the streptococci but enough to educate them to resist penicillin. He then infects his wife. Mrs. X gets pneumonia and is treated with penicillin. As the streptococci are now resistant to penicillin the treatment fails. Mrs. X dies. Who is primarily responsible for Mrs. X's death? Why Mr. X whose negligent use of penicillin changed the nature of the microbe. Moral: If you use penicillin, use enough.

It is not difficult to make microbes resistant to penicillin in the laboratory by exposing them to concentrations not sufficient to kill them, and the same thing has occasionally happened in the body.

The time may come when penicillin can be bought by anyone in the shops. Then there is the danger that the ignorant man may easily under-dose himself and by exposing his microbes to non-lethal quantities of the drug make them resistant."

— Alexander Fleming

Nobel Lecture, December 11, 1945, Sweden

Antimicrobial resistance: a global threat

Antimicrobial resistance (AMR) represents one of the most pressing existential threats to global public health, occurring when bacteria, viruses, fungi, and parasites evolve to withstand the drugs designed to eliminate them, rendering standard treatments ineffective and infections increasingly lethal.[1] This crisis was presciently predicted by Alexander Fleming in his 1945 Nobel lecture.[2] His prophecy has materialized with devastating precision: the WHO surveillance data in 2014 reveals that over 50% of pathogenic bacteria causing common infections: including *Escherichia coli* and *Staphylococcus aureus*, now exhibit reduced susceptibility to antibiotic treatments in both hospital and community settings (Fig. 1).[3] The follow-up report in 2019 is staggering: bacterial AMR directly caused 1.27 million deaths globally in 2019 and contributed to 4.95 million fatalities, surpassing the combined mortality of HIV/AIDS and malaria, with projections suggesting 10 million annual deaths by 2050 if current trajectories persist (Fig. 1).[3,4]

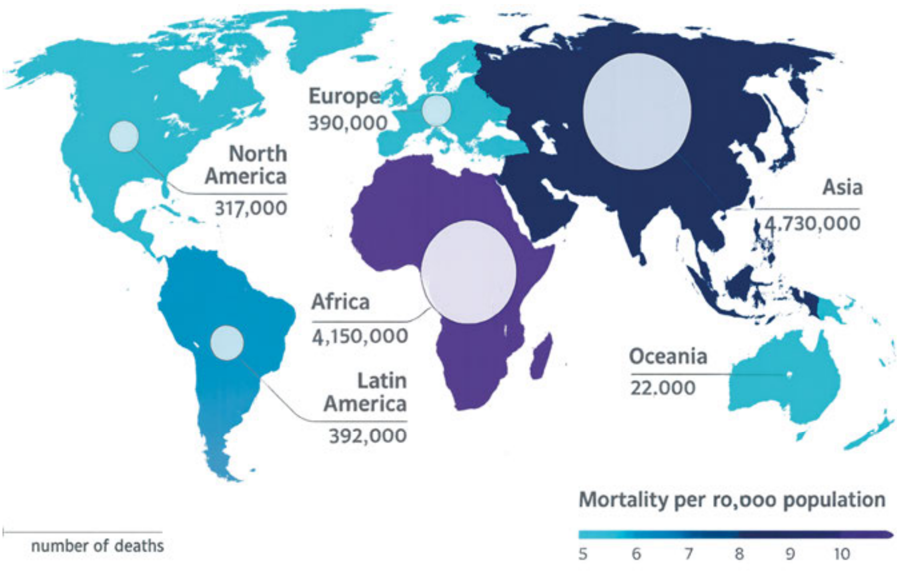

Figure 1. Deaths attributable to antimicrobial resistance every year by 2050, predicted by Review on Antimicrobial Resistance: Tackling a Crisis for the Health and Wealth of Nations. 2014, with permission from review on: *Antimicrobial Resistance. Antimicrobial Resistance: Tackling a Crisis for the Health and Wealth of Nations. 2014.*

The demand for new and efficient treatments has thus become not merely urgent but existential: a necessity for treating bacterial infections, large or small, in the immediate future.

Current challenge of making antibiotics for oral delivery

Oral administration for antibiotic therapy is preferred by most of patients for its non-invasiveness, cost-effectiveness and superior patience.[5] Most antibiotics suffer from physicochemical limitations: poor solubility, low intestinal permeability, and rapid enzymatic degradation in the GIT.[6] To achieve MIC at systemic infection sites, physicians must prescribe oral doses much higher than theoretical requirements, with some antibiotics requiring gram-level daily dosing. This excessive exposure to the GIT can adversely affect the gut microbiota, potentially increasing the development of bacterial resistance and the risk of infections by opportunistic pathogens.[7]

Formulating drugs with poor oral bioavailability into lipid-based nanocarriers has emerged as an attractive strategy to increase drug absorption while simultaneously enhancing solubility and chemical stability (Fig. 2).[6] There are multiple kinds of nanoparticles applied with oral delivery (Fig. 2). Currently, the majority of clinically approved lipid-based antimicrobials consist of liposomal formulations, including AmBisome®, Arikayce®, and Abelcet®, which have achieved significantly reduced toxicity compared to conventional formulations.[8,9]

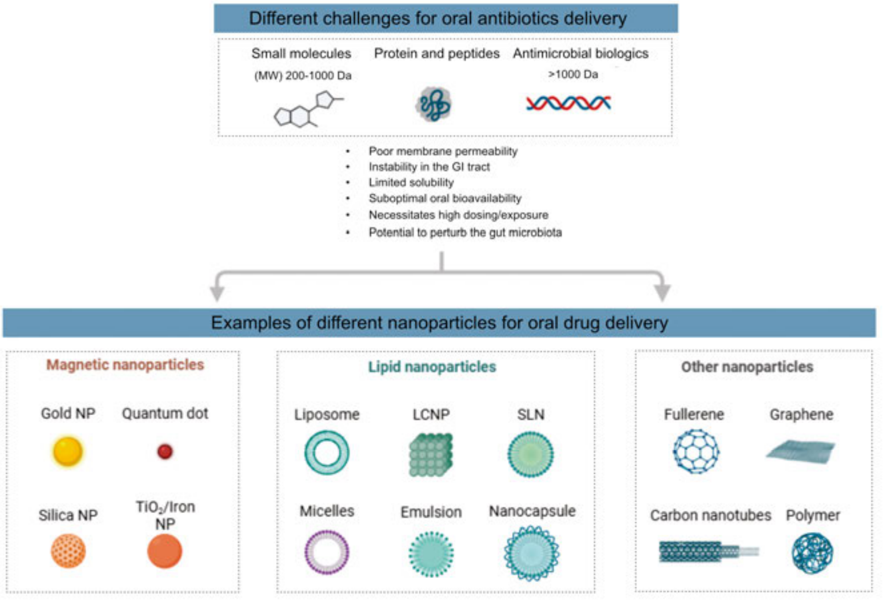

Figure 2. Challenges of antibiotics for oral delivery nanoparticles. Upper panel: Antibiotics can be broadly divided into small molecules, proteins, and antimicrobial biologics. Lower panel: Examples different nanomaterials.

However, despite these achievements in parenteral applications, conventional liposomal systems face several critical limitations when adapted for oral drug delivery.[10] Furthermore, there have been no liposomal formulations approved for oral use to date, despite the success of parenteral liposomes. This translational gap between successful parenteral liposomal formulations and the unmet need for oral delivery systems necessitates the development of next-generation nanoparticles specifically engineered to survive the GI environment.

Liquid crystal nanoparticles

Advancements in the field of non-lamellar liquid crystal nanoparticles (LCNPs) have accelerated the progress of lipid nanoparticle-mediated drug delivery.[11–13] Lyotropic LCs are a subclass of LC obtained when amphiphilic molecules are dissolved in a suitable solvent.[14] To understand which phase will be formed upon dissolving amphiphilic molecules, Israelachvili et al.[15] proposed a CPP theory. In this model each individual amphiphilic molecule is represented by cone-like structure, which assemble into micelles through self-assemble. The CPP can be calculated using

$$CPP = \frac{v}{a \cdot l}$$

where v describes the volume of the conical micelle, a is the area and l is the height of the cone. For CPPs < $\frac{1}{3}$ spherical micelles are formed, whereas the LC will exhibit cylindrical micelles for $\frac{1}{3}$ < CPP < $\frac{1}{2}$. Lamellar structures possess a CPP around 1 and CPPs > 1 result in inverted structures (cylindrical or spherical).[16]

The amphiphilic lipids that constitute LCNPs self-assemble into diverse internal nanostructures with varying mesophases and curvatures, ranging from lamellar bilayers to complex non-lamellar architectures including primitive cubic (Im3m), diamond cubic (Pn3m), gyroid cubic (Ia3d), and inverse hexagonal (H_{II}) phases.[11,12,17,18] Cubosomes are LCNPs with an internal bicontinuous cubic (Q_{II}) phase and consist of a single lipid bilayer that forms a continuous periodic membrane lattice structure with pores formed by two interwoven water channels (Fig. 3).[12]

Hexosomes, on the other hand, are defined by an inverse hexagonal (H_{II}) phase and form rod-shaped inverse micelles, organized in a hexagonal structure with closed water channels.[19] This structural versatility shapes into distinct physicochemical properties that enable broad therapeutic applications for multiple drug delivery. LCNPs have demonstrated utility in oral delivery of poorly absorbed drugs such as insulin, VAN and CLA, where their unique internal architecture enhances GI stability. [20–22]

Also, In vaccine delivery, topical and intravenous delivery, they serve as effective carriers for RNA[23,24], ovalbumin (OVA)[25,26] and amino acids[27,28], providing immunostimulatory effects alongside antigen protection (Figure 3).[20–32]

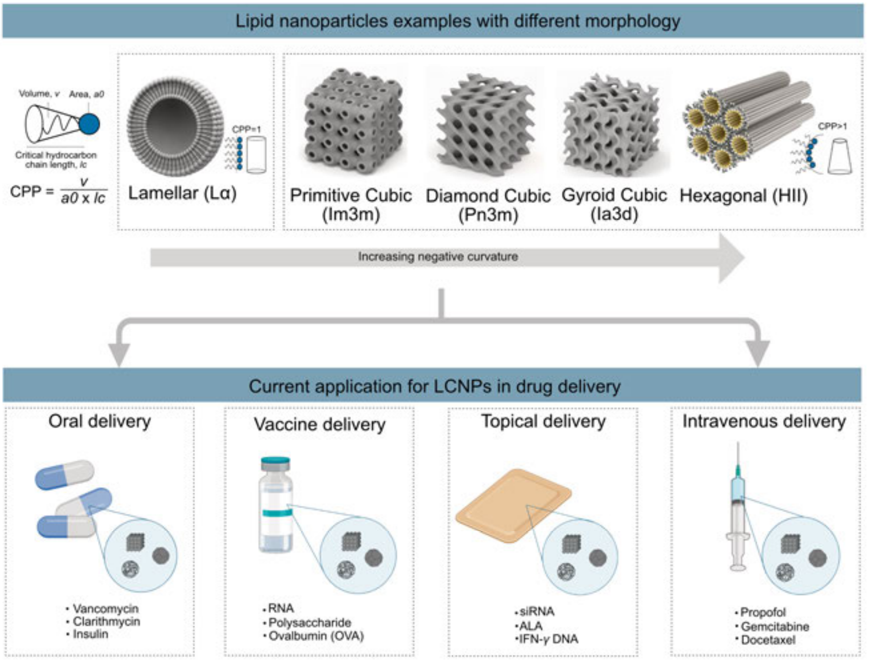

Figure 3. Illustration of lipids with different critical packing parameters and how they inform the liquid crystal phase of self-assembled lyotropic liquid crystals and examples of current application for LCNPs in drug delivery. Parts of the figure is created with Biorender.

Preparation and rational design of LCNPs

LCNPs can be prepared through three primary approaches, each offering distinct advantages and limitations for pharmaceutical applications.[33–38] Ultrasonication of bulk liquid crystalline gels represents a straightforward technique that reduces particle size and produces relatively narrow size distributions, typically yielding particles in the 100-200 nm range.[34]

However, the high-energy input generates localized heating that may cause degradation of thermally sensitive drugs, and potential contamination from probe erosion remains a concern. Microfluidic preparation methods provide highly reproducible and scalable production with precise control over formulation parameters such as flow rates and lipid ratios, making them advantageous for industrial translation.[37,38]

The main drawbacks include higher initial capital costs, requirement for specialized equipment like microfluidic chips, and reduced efficiency when processing highly viscous lipid formulations.[38] The hydrotrope method involves diluting an isotropic lipid-ethanol mixture with aqueous stabilizer solution, offering accessible laboratory-scale preparation with low energy consumption and suitability for hydrophobic drugs.[36] This approach, however, necessitates organic solvents as hydrotropes and typically generates larger particles (>200 nm) with broader, potentially polydisperse size distributions.[36]

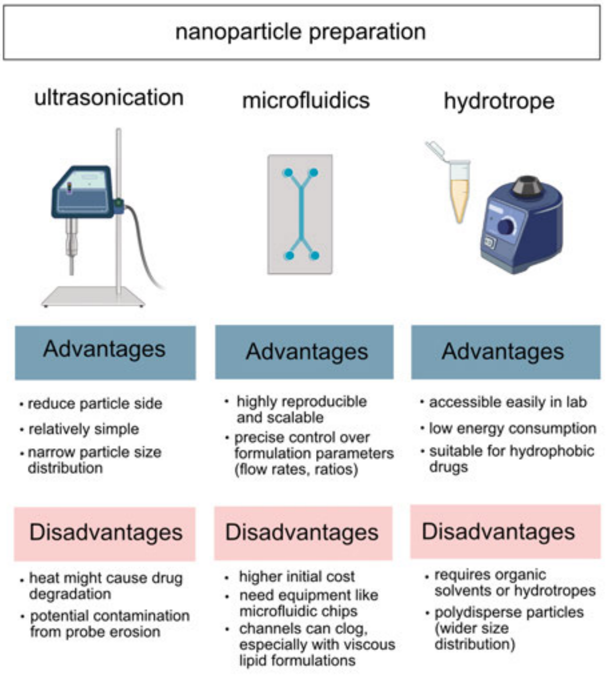

Figure 4. Illustration of different common preparation methods and sterilization methods. Parts of the figure is created with Biorender.

All three preparation methods require the incorporation of stabilizers to produce stable LCNP dispersions, with Pluronic F127 being the most commonly employed amphiphilic block copolymer.[39,40] F127 plays a multifunctional role in LCNP formulation: it adsorbs onto particle surfaces to provide steric stabilization, preventing aggregation during storage and biological application.

It is also crucial to note that the choice of lipid also significantly influences LCNP stability.[41,41] Some lipids contain ester-link such as glyceryl monooleate (GMO) exhibit rapid degradation by pancreatic lipase, leading to a limited capacity to enhance oral absorption.[17,21,22] On the other hand, lipids lacking ester functional groups, such as oleyl glycerate[17], phytantriol (PHY)[22,42], and selachyl alcohol(SA)[43], sustain the absorption of poorly soluble drugs after oral administration. Therefore, the digestibility of glyceride-based lipids with ester groups emerges as a general limitation, impacting LC structure and, consequently, oral drug absorption.[17] This aspect needs careful consideration during the formulation design process.

PHY alone spontaneously forms a bicontinuous cubic phase (Pn3m) in excess water. α-Tocopherol (TOC) and farnesol (FAR) both have large lipid tail that preferentially partition into the hydrophobic interior of the lipid bilayer, as shown in Figure 5. The addition of TOC or FAR increases the CPP of the lipid mixture by enlarging the hydrophobic chain volume.[22]

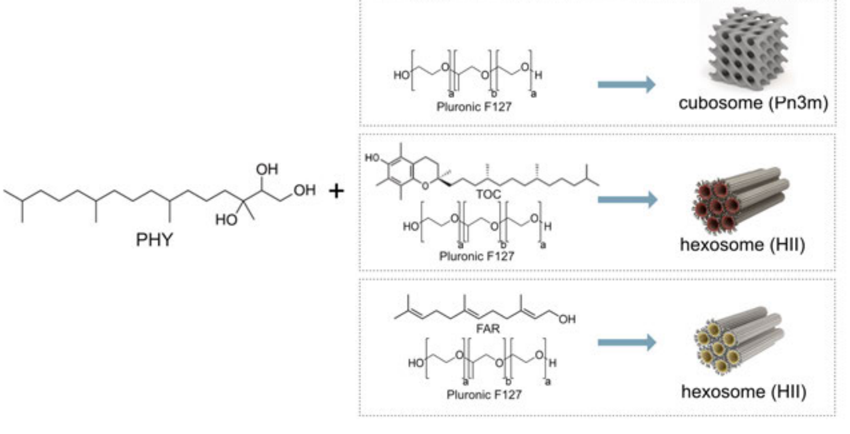

Figure 5. Illustration of incorporation different lipids into PHY modulates liquid crystal phase behavior.

Drug loading and partitioning of LCNPs

Unlike conventional liposomes, which encapsulate a single aqueous core, LCNPs offer a significantly higher surface area-to-volume ratio through their water channel, enhancing their ability to encapsulate and deliver both hydrophilic and hydrophobic antibiotics. Table 1 provide an overview of small molecule antibiotics.[22,44–59] Table 2 provide some example of antimicrobial peptides, respectively.[22,60–70]

These studies report encouraging outcomes including enhanced encapsulation efficiency and controlled release kinetics (rifampicin, in vitro), improved mucosal and ocular retention and permeation (ciprofloxacin and moxifloxacin, in vitro and in vivo), enhanced biofilm penetration and eradication (gentamicin and tobramycin, in vitro and in vivo, including nebulized delivery), oral sustained-release properties (clarithromycin, in vitro and in vivo).[22,44,46,58]

Also, in terms of protection from proteolytic degradation (LL-37 topical gel, ex vivo, pig-skin model), enhanced cellular uptake and intracellular bacterial clearance (cationic vancomycin cubosomes, in vitro, macrophages/epithelia), preserved activity after lyophilization and rehydration (AP114 hexosomes, in vitro), high encapsulation with controlled release (indolicidin, in vitro), protein-corona guided targeting while retaining Gram-negative activity (LL-37, in vitro, serum), and synergy via polytherapy (polymyxin B + blank cubosomes, in vitro, MDR Gram-negatives).[62–64,70]

Table 1 Examples of LCNPs loaded antibiotics for drug delivery (small molecule)

Antibiotic	MW (g/mol)	Primary Component	EE%	Bacterial Model	Administration	Applications/Efficacy	Ref.
Gentamicin	477	PHY; GMO; + Pluronic F127	95%	*Escherichia coli (E. coli)* planktonic & biofilm	NR	Enhanced antibiofilm efficacy vs E. coli	58
Tobramycin	467.5	Monoolein (digestible LCNPs) + Pluronic F127	High (>90%)	*P. aeruginosa biofilms*	NR	100-fold improvement over free antibiotic; complete eradication	49,66
Amikacin	585.6	PHY	NR	NR	NR	Enhanced biofilm penetration potential	65
Gallium Protoporphyrin	651.3	GMO + Pluronic F127	98.2±3.2%	*S. aureus*	Photodynamic therapy	MIC = 0.125 μg/mL, first lyophilized LCNP	48
Amoxicillin	365.4	MO; GMO + Pluronic F127	High	*S. aureus*	Topical delivery	Greater antibacterial effect vs free drug	47
Gemifloxacin	389.4	GMO	NR	*Methicillin-Resistant Staphylococcus aureus (MRSA)*	Ocular delivery	Enhanced performance via glyceryl monooleate cubosomes	24
Gatifloxacin	375.4	GMO,Poloxamer 407 (P407)	52.8% ± 2.93	*MRSA*	NR	Enhanced performance	49
Norfloxacin	319.3	GMO	NR	NR	Topical delivery	Lower MW enables high drug loading,enhancing the management of otitis externa.	47
Dapsone	248	GMO + Poloxamer 407	> 84.3 ± 2.7	NR	Topical delivery	Increased permeation of drug across the skin	45
Ciprofloxacin	331.3	GMO + Poloxamer 407	75%	*S. aureus*	Topical delivery	Improved corneal permeation and prolonged ocular retention	46
Azithromycin	749	GMO + Pluronic F127	74-88%	*Periodontitis rat model*	Local periodontal	Sustained release; reduced dosing vs marketed gel	56
Clarithromycin	748	GMO; PHY; PHY/TOC; PHY/FAR; + Pluronic F127	96.80 ± 1.50 %; >90%	*Pseudomonas aeruginosa, Escherichia coli, Bacillus subtilis, and Staphylococcus aureus*	Oral delivery	Anti-biofilm, anti-inflammatory activities; protection of get commensal bacteria	22,44
Erythromycin	734	GMO + Poloxamer	95.29±1.32 %	*Acne treatment*	Topical delivery	75% release in 7h, enhanced skin penetration	57
Rifampicin	822.9	GMO	NR	*MRSA (S. aureus)*	NR	Lowered MIC vs free rifampicin via LCNP delivery	71
Tetracycline	444.4	GMO	95.46 ± 4.13 %	NR	Ophthalmic deliver	increasing the ocular bioavailability of TET by enhancing its retention time and permeation into the cornea.	52
Delamanid	534.5	PHY; SA + Pluronic F127	NR	NR	Oral delivery	sustained oral absorption vs PHY; prolonged exposure supportive of depot-like release	55
Chloramphenicol	323.1	GMO ± Poloxamer (F127/P407)	NR	NR	Topical delivery	Sustained release from cubic matrices with improved local delivery versus free drug	60

Table 2. Examples of LCNPs loaded antibiotics for drug delivery (large molecules or peptides)

Drug	MW (g/mol)	Primary lipid	EE%	Bacterial model	Administration	Key findings	Ref.
Vancomycin (glycopeptide)	1449	GMO/MO; PHY; PHY/TOC; PHY/FAR; + Pluronic F127	95.4% to 100.6%; >90%	*MRSA, Escherichia coli, Enterococcus*	Ocular delivery; Oral delivery; Intrevenous Delivery	Successfully loaded despite MW >1000 Da; retained antimicrobial activity; non-digestable LCNPs protect commensal bacteria Cationic cubosomes achieved high uptake into host cells and reduced intracellular bacterial	22,60,61
LL-37 (cathelicidin)	4493	GMO + Pluronic F127	NR	*P. aeruginosa, S. aureus* (planktonic + biofilm); *E. coli; A. Baumannii*	Topical delivery	Encapsulation reduced LL-37's Gram+ activity but retained Gram– activity; cubosome protected LL-37 from proteolysis, improved bacterial kill in pig wound model; killing; cubosomes paradoxically increased S. aureus biofilm biomass	62,63,64
DPK-060 (kininogen-derived AMP)	2503	GMO	50–70%	*S. aureus, E. coli*	NR	Cubosome formulations retained DPK-060 activity, while hexosome encapsulation reduced efficacy	65
AP114 (plectasin derivative)	4410	GMO	NR	*S. aureus*	NR	Rehydrated AP114-LCNPs formed stable hexosomes with preserved activity; trehalose formulation maintained size and maximized antibacterial activity	66
Indolicidin (AMP)	1900	PHY + Pluronic F127		*E. coli, MRSA (S. aureus)*	NR	Successfully loaded with high EE in high-salt prep, but encapsulation did not enhance efficacy compares to free drug	67
Indolicidin analog ('Priscilicidin')	2000	PHY +Pluronic F127	High	*E. coli, MRSA (S. aureus)*	NR	Ultra-short indolicidin analog loaded with high EE but no significant efficacy improvement compares to free drug	68
Polymyxin B	1203	PHY + Pluronic F127	NR	*A. baumannii, P. aeruginosa, K. pneumoniae*	NR	cubosomes achieved high EE but modest MIC improvement. Polytherapy (drug + blank cubosomes) enhanced killing Gram-negatives	69
Colistin (polymyxin E)	≈1155	Phytantriol (PHY) + Pluronic F127	NR	*A. baumannii, P. aeruginosa, K. pneumoniae*	NR	LCNP platform enhanced activity of the aminoglycoside class and colistin compares to free drug	70

Many studies have loaded diverse antibiotics into LCNPs and explored various applications; however, the fundamental determinants of release, drug partition coefficient, drug lipid interactions, and diffusion within the nanostructured bilayer remain insufficiently characterized. Although prevailing studies point to partitioning and intramembrane diffusion as the primary drivers of release, the field is still, in many respects, operating without clear mechanistic guidance.[12]

In practice, drug release from LCNP dispersions is typically assessed by diluting the dispersion and quantifying subsequent transfer of drug into the surrounding medium, using a range of techniques (Figure 6).[72–74] Among these, pressure ultrafiltration has been highlighted as particularly useful because it allows direct dilution into physiologically relevant media while minimizing membrane-transport artifacts (demonstrated for gentamycin, rifampicin, and vancomycin).[22,58,72,75] Yet, there is no consensus on the optimal approach for specific cases.

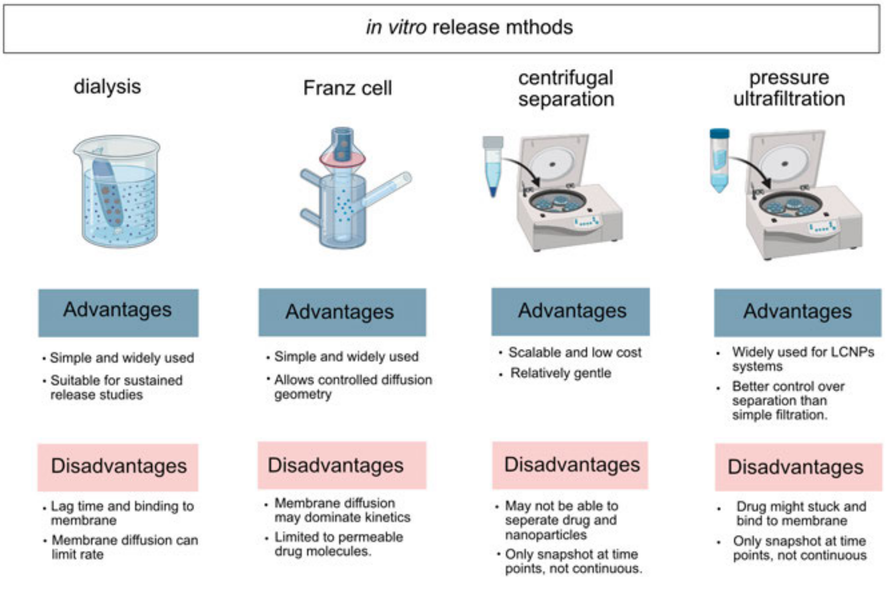

Figure 6. Illustration of different common *in vitro* release methods. Parts of the figure is created with Biorender.

Currently, most studies indicate that for hydrophobic molecules, release mechanisms are primarily governed by the partition coefficient between the lipid bilayer and the aqueous phase, intramembrane diffusion rates, and subsequent partitioning into the surrounding medium.[76,77] In contrast, hydrophilic cargo release is driven by diffusion through aqueous channels, owing to their higher water affinity.[77,78] Other physicochemical properties of the cargo, such as size, charge and environmental factors including temperature, pressure, and pH, also play significant roles.[12]

Cellular uptake of LCNPs

For LCNPs, uptake mechanisms can dictate not only the extent of drug absorption but also intracellular trafficking, efflux, and eventual bioavailability. Drug transport across the intestinal epithelium is a highly orchestrated process, governed by a complex interplay of passive diffusion and endocytic vesicular trafficking.[79] For nanocarriers such as LCNPs, uptake mechanisms can dictate not only the extent of drug absorption but also intracellular trafficking, efflux, and eventual bioavailability. Existing studies, largely conducted on non-intestinal or immortalized cancer cell lines, suggest that LCNPs may leverage multiple endocytic routes, including clathrin-mediated endocytosis, macropinocytosis, as well as non-endocytic interactions such as direct lipid membrane fusion or phase-through.[80–87] (Fig. 7)

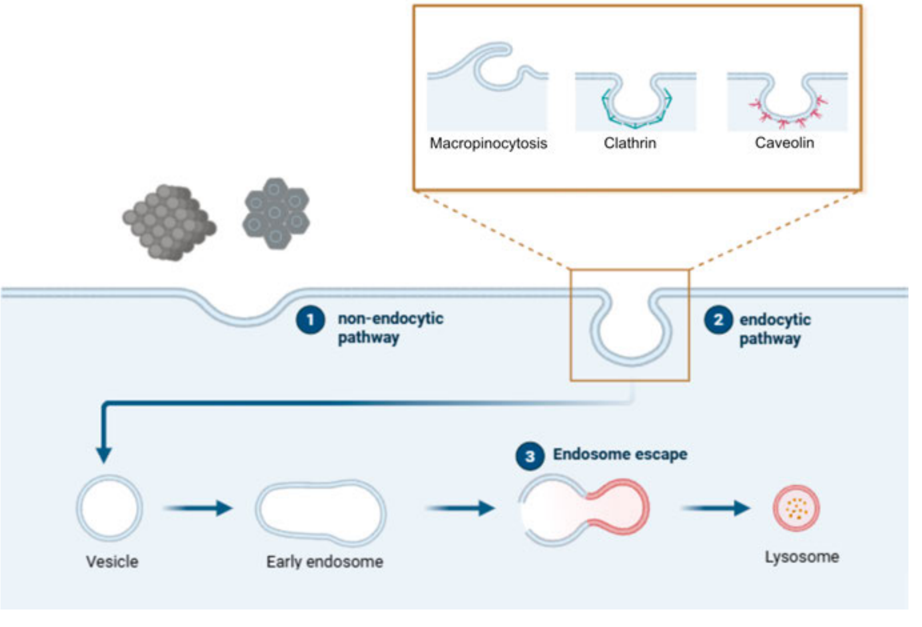

Figure 7. Illustration of simplified cellular uptake via non-endocytic mechanisms (left) and endocytic internalization (right). Parts of the figure is created with Biorender.

While these findings have provided valuable initial insights, they remain somewhat limited by choice of model and often lack validation in physiologically relevant intestinal systems. In particular, the relative contributions of distinct uptake pathways appear highly sensitive to LCNP physicochemical attributes such as surface area, fusogenicity, particle size, surface charge, lipid composition, and the presence of targeting moieties. For example, neutrally charged LCNPs of around 150 nm are sometimes reported to favor clathrin-mediated uptake, while cationic or larger particles may rely partially on macropinocytosis or dominantly on fusion-based mechanisms.[88,89] Yet, these trends lack robust experimental confirmation in relevant intestinal epithelial models such as Caco-2 model.

Solid LCNP formulations via 3D printing

To broaden LCNP applications, solid formulations offer advantages for long-term stability, drug transportation, and customized dosing efficiency. LCNP-forming solid systems capable of in situ transformation upon oral administration are easier to handle than liquid dispersions and provide superior chemical stability for peptide antibiotics by preventing hydrolytic degradation.[39,75,90]

3D printing technology enables precise manufacturing of LCNP-containing solid dosage forms with controlled dose, geometry, and release profiles. Semi-solid extrusion (SSE) is particularly suited for pharmaceutical LCNP applications, operating by depositing gel materials in sequential layers through pneumatic, piston, or screw-driven systems (Figure 8).[91] SSE can be performed at ambient temperature, preserving thermally sensitive LCNPs and antibiotics while accommodating nanostructured gel formulations with direct API incorporation.[91] Key advantages include dose flexibility for narrow therapeutic index antibiotics, personalized dosing for specific patient populations, multi-drug integration with independent release profiles, and precise spatial API distribution.[91–95]

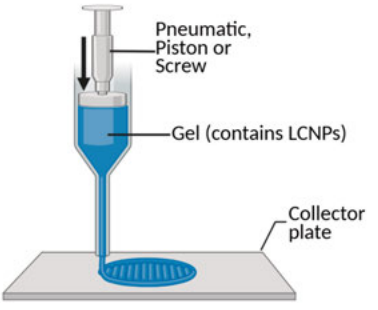

Figure 8. SSE 3D printing using pressurized air. Figure is created from Biorender.

However, research on 3D-printed LCNP systems remains limited. Few studies focus on bulk LC rather than LCNP dispersions, leaving critical questions unaddressed: nanoparticle structural stability during extrusion, uniformity of printed tablets, and drug content accuracy. Further investigation is needed to establish manufacturing parameters and quality standards for clinical translation.[39,75,90,95]

Challenges of LCNPs as oral delivery formulation

LCNPs offer a potentially transformative approach to oral antibiotic delivery, yet their clinical development lags far behind their theoretical promise. Early proof-of-concept studies have proved improved solubility and bioavailability gains for several antibiotics but these reports rarely probe the underlying release and cellular uptake mechanisms.[20–22,75,90] Critical questions remain unanswered: How do LCNPs interact with different drugs? Which cellular uptake pathways do they exploit? How do they influence oral absorption, release kinetics, and *in vivo* pharmacokinetics? Once an antibiotic is administered orally within an LCNP formulation, we cannot clearly determine its exposure to the gut microbiota, its release behavior, the epithelial uptake and endocytic routes it engages, or how efficiently the active drug ultimately reaches the systemic circulation. Without clarifying these mechanistic contributions, formulation design risks remaining empirical rather than rational, thereby slowing optimization and delaying clinical translation.

Aim

This thesis presents a pipeline from molecular understanding to practical manufacturing through four interconnected studies: (1) development and characterization of antibiotic-loaded LCNPs with validated stability and protective effects for model commensal bacteria, (2) molecular dynamics simulations revealing cargo-LCNP interactions and release mechanisms, (3) investigation of cellular uptake mechanisms and transepithelial permeability across different mesophases, and (4) integration of LCNPs with 3D printing for scalable, personalized dosage form. Together, these studies establish a framework for next-generation oral antibiotic delivery systems that combat antimicrobial resistance through improved accessibility and patient compliance.

- To develop novel oral formulations capable of overcoming these barriers, thereby combination enabling efficient and practical antibiotic delivery. (Paper I).
- To elucidate drug loading, localization, and release mechanisms in hexagonal phase (H_{II}) LCNPs for improved oral antibiotic delivery. (Paper II).
- To evaluate how different internal mesophases of LCNPs influence transepithelial transport and enhances the oral permeability of vancomycin compared to conventional liposomes. (Paper III).
- To develop a scalable, modular platform for producing personalized oral vancomycin (VAN) tablets by combining liquid crystal nanoparticles (LCNPs) with semi-solid extrusion (SSE) 3D printing, enabling improved delivery of poorly bioavailable antibiotics. (Paper VI).

Method

Preparation of cubosomes, hexosomes and liposomes

In paper I, II, III, and IV, to prepare cubosome and hexosomes, PHY (100 mg) alone for (cubosome); PHY (80 mg) and TOC (20 mg) or PHY (90 mg) and FAR (10 mg) for hexosomes were weighed and melted homogeneously. A Pluronic® F127 solution in water (10 mg/mL) was added to the PHY/TOC or PHY/FAR lipid mixture (total lipid concentration of 100 mg/mL), followed by intense vortexing and agitation at 70°C and 3500 rpm for 40 min (ThermoMixer, Eppendorf, Schönenbuch, Switzerland). The mixtures were treated with 10 min of ultra-sonication at 1 s pulse, 1 s pause with 40% amplitude (SonicsVCX 750 with microtips 630-0423) to give a milky dispersion. Finally, the samples were kept in glass vials at room temperature for equilibration (one week) until further characterization. For the liposome preparation, 4 mL of DOPC (25mg/mL in chloroform) were transferred to a glass vial and the chloroform was first slowly evaporated using a gentle stream of nitrogen gas to produce a thin lipid film. The thin lipid film was then left to dry in a vacuum oven (Vacutherm, Thermo Fisher scientific, Sweden) at 45°C overnight. To disperse liposomes, the lipid layer was rehydrated with Pluronic® F127 aqueous solution (10 mg/mL) to achieve a total lipid concentration of 100 mg/mL and sonicated in a bath sonicator (Elmasonic S 40 H ultrasonic bath (Elma Schmidbauer GmbH, Singen, Germany) at 60°C for 30 min. The lipid nanoparticles used in each paper are summarized in figure 9.

composition	Paper I	Paper II	Paper III	Paper IV
PHY + F127				
PHY/TOC + F127				
PHY/FAR + F127				
DOPC + F127				
VAN loaded	✓	✓	✓	✓
CLA loaded	✓	✓		

Figure 9. Overview of the lipid nanoparticles produced in Papers I-IV.

Characterization of lipid nanoparticles

Encapsulation of antibiotics

In paper I, III and IV, drug encapsulation efficiency (EE%) was determined indirectly by separating encapsulated VAN or CLA from the non-encapsulated fraction using ultrafiltration centrifugation.[72] Briefly, a 0.5 -2 mL aliquot of the lipid nanoparticle was centrifuged using an Amicon® Ultra-2 centrifugal filter (Merck, Darmstadt, Germany) with a 50,000 Da molecular weight cut-off (MWCO) at 25 °C, following the manufacturer's instructions. The concentration of non-encapsulated VAN and CLA in the filtrate was determined with Ultra Performance Liquid Chromatography (UPLC) (HPLC ELITE LaChrom VWR HITACHI, Solna, Sweden) with UV detector Hitachi L-2400. The encapsulation efficiency (EE) was calculated as follows:[96,97]

$$EE\ \% = 1 - \left(\frac{Amount\ of\ free\ drug}{Total\ amount\ of\ drug} *\ 100\%\right)$$

Dynamic light scattering (DLS)

In paper I, III, IV, particle size and zeta potential (ZP) analyses were performed using a Litesizer 500 (Anton Paar GmbH, Graz, Austria) dynamic scattering instrument. Samples were diluted (1:200) in water or cull culture whole medium and measured in disposal cuvettes (BRAND™ four-clear sided disposable polystyrene cuvettes, Brand, Wertheim, Germany) and omega cuvette (Anton Paar GmbH) for the determination of size and ZP, respectively. All measurements were performed in triplicate at 25°C after 1 min equilibration using Smoluchowski approximation and Henry Factor of 1.5. The data were processed with the Kalliope software (Version 2.12.1, Anton Paar GmbH).

Small-angle X-ray scattering (SAXS)

In paper I, II, III and IV, SAXS measurements were performed on a Xeuss 2.0 Q-Xoom system (Xenocs, Grenoble, France) equipped with a GENIX 3D Cu Ultra Low Divergence (λ = 1.54 Å) X-ray source and a two-dimensional PILATUS 3R 300K X-ray Detector (DECTRIS AG, Baden-Daettwil, Switzerland). For the characterization of the particles in paper I, II and III, the dispersions were introduced into glass capillaries (1.5 mm light path, Wjm - Glas Müller GmbH, Berlin, Germany), which were then sealed with epoxy glue. In paper IV, the gel, fresh/dried tablet, and rehydrated tablet were placed between two Kapton films mounted in a Xenocs vacuum-sealed gel holder (Xenocs, Grenoble, France). Samples were allowed to equilibrate for at least 24 hrs prior to analysis. The sample-to-detector distance was 401 mm with an acquisition time of 30 min. A silver behenate sample was used for calibration. A pin diode was used to measure the transmission of the sample. Scattering 2D images were reduced to 1D curves, normalized to an absolute scale, and the buffer and cell scatterings were subtracted from the sample scattering using the Foxtrot software package (XSACT 2.4, Grenoble, France).

Cryogenic transmission electron microscopy (cryo-TEM)

In paper I, III and IV, for cryo-TEM sample preparation, 4 µL of each sample was applied to R2/1 300 mesh glow discharged grids (Quantifoil Micro Tools GmbH, Großlöbichau, Germany) and thereafter vitrified using a Vitrobot MkIV (Thermo Fisher Scientific) set to 22°C, using a blotting time of 3 s and waiting time of 15 s. Cryo-TEM images were acquired on a Glacios microscope (Thermo Fischer Scientific) fitted with a Falcon 4i direct electron detector operated at 200 kV. All images were taken at a nominal magnification of 45k, corresponding to a pixel size of 3.1 Å/px using a total electron dose of 10 e/A^2 and 4 µm defocus.

Stability studies

In paper I, all LCNP formulations were stored at room temperature for 28 days. Physicochemical characteristics for stability test such as particle size, polydispersity, ZP, and EE% were determined as described above at specific intervals. Prior to each evaluation, all the LCNPs were vortexed to ensure proper dispersion and consistency in the measurements.

Small-volume in vitro lipolysis

In paper I, *in vitro* lipolysis experiments were conducted according to a standardized method using a small-volume temperature-controlled glass vessel (20 mL, Metrohm AG, Herisau, Switzerland). The system comprised a pH electrode (Biotrode, Metrohm AG) coupled to a dosing unit (907 Titrando, Metrohm AG).[98] For the lipolysis experiment, 200 mg of each LCNP formulation was first dispersed in digestion medium (9 mL) under constant stirring at 450 rpm in a temperature-controlled glass vessel (37°C). After 10 min, 888 µL of pancreatic extract was added to initiate digestion. A 0.2 M NaOH solution was used as titrant to keep pH stable at 6.5 by autotitration during the digestion process. The extent of lipolysis (%) was calculated using previously described method:

$$Lipolysis\ \% = \frac{ionized\ FAs}{theoretical\ FAs\ in\ LCNPs} * 100$$

where the amount of ionized fatty acids (FAs), which is derived from the NaOH volume used during titration, is correlated to the theoretical number of FA that can be released from lipids within the LCNPs during the *in vitro* digestion. The samples were diluted with either acetonitrile for CLA or water for VAN for HPLC analysis (described below). *In vitro* lipolysis experiments were replicated three times.

In vitro release

In paper I and II, to determine the drug release from the nanoparticle systems, a volume of 50 µL of each LCNPs dispersion was used to separate free drug from LCNPs following the centrifugation procedure described above (encapsulation of antibiotics). A volume of 0.9 mL of PBS (pH 7.4) was then added to the LCNPs loaded with antibiotics and shaken at 120 rpm at 37°C (Incubating Microplate Shaker, VWR, Stockholm, Sweden). At predefined times the solution was centrifuged at 3500 rpm for 5 min (room temperature) and 0.9 mL of the supernatant were carefully collected and replaced by 0.9

mL of fresh PBS.[72] The collected part was analyzed by HPLC to determine the concentration of drug at each time point. The experiment was performed in triplicate. With the drug concentrations estimated, the cumulative drug release was calculated at each time point with the following formula:

$$Cumulative\ Release = \left(\frac{Amount\ of\ drug\ release}{Total\ amount\ of\ drug}\right) * 100\%$$

where the amount of drug released in the medium is the concentration of drug at any time multiplied by the volume of medium and the total amount of drug loaded in the nanoparticles is the amount of the drugs loaded in the LCNPs.

High performance liquid chromatography (HPLC)

In paper I, II, III, and IV, drug concentration was determined using a HPLC (LaChrom VWR HITACHI, Solna, Sweden) with UV detector Hitachi L-2400, Anaheim, USA) with a ZORBAX Eclipse XDB-C18 Rapid resolution column (4.6 x 100 mm, 3.5 µm). The mobile phase isocratic elution acetonitrile and sodium acetate buffer (pH = 5.0) with ratios of 60:40 for CLA and 8:92 for VAN with a flow rate of 1.0 mL/min and a 20 µL injection volume. The column was maintained at 40°C, and detection occurred at 230 nm for VAN and 205 nm for CLA using a UV detector. Data was processed using Agilent EZChrom Elite software (version 3.3.2 SP2, Agilent Technologies, Santa Clara, CA, USA).

Diffusion ordered spectroscopy (DOSY)

In paper I, to confirm drug entrapped by LCNPs, nuclear magnetic resonance (NMR) spectra were recorded at 37°C on a 600 MHz Bruker Avance Neo Spectrometer equipped with a TCI cryogenic probe. DOSY spectra was measured with a gradient pulse length of 0.8 ms and a diffusion time of 200 ms. Gradient strength in the analyzed data varied, over 16 DOSY slices, from 2% to 98% of 6.51933 gauss/mm. 1H NMR spectra for pure VAN and CLA samples in 90% H2O + 10% D2O were obtained with water suppression using excitation sculpting with gradients. 1H NMR spectra for all LCNP formulations in 90% H2O + 10% D2O were obtained using "zgesgp" for selective excitation of water resonance. DOSY spectra of the samples were recorded with ledbpgp2s pulse sequence with excitation sculpting to suppress water. Finally, all NMR data were analyzed using Bruker Topspin (4.3.0 version). The diffusion coefficient was calculated by eq:

$$I = I0\ \exp\left(-\gamma^2 * s^2 * g^2 * \delta^2\left(\Delta - \frac{\delta}{3} - \frac{\tau}{2}\right)D\right)$$

where γ represents the gyromagnetic ratio of protons, and s, g, δ and Δ denote the shape factor, gradient amplitude, gradient pulse length, and diffusion time, respectively, for a single pair of gradient pulses. Additionally, τ is the interval within the bipolar pulse pair.

Minimum inhibitory concentration (MIC) and broth microdilution (BMD) assay

In paper I, to validate the protective function of LCNPs to representative gut bacteria. MIC tests were carried out through the BMD assay reference method in accordance with European Committee on Antimicrobial Susceptibility Testing (EUCAST) guidelines (version 14.0). Antibiotic-loaded LCNPs formulations were diluted in MHB and dispensed into 96-well microtiter plates at an initial concentration of 1024 mg/L, followed by a 10-step two-fold dilution in MHB. Fresh bacterial colonies of *Escherichia coli* ATCC 25922 (Gram-negative) and *Enterococcus faecalis* ATCC 29212 (Gram-positive) on MHA were suspended in 0.9% NaCl to a density of 1×10^8 CFU/mL. The suspension was diluted in MHB to a concentration of 1×10^6 CFU/mL. Suspensions were added to each well, reaching a final bacterial concentration of 5×10^5 CFU/mL. Each microtiter plate contained growth controls and media controls. All the proper technical controls were included (sterility, DMSO, MIC of blank LCNPs). All compounds were tested in biological duplicates (derived from different colonies) and results were only accepted if duplicates did not deviate more than one dilution. Co-administered and dual loaded LCNPs were compared to a non-formulated mixture of VAN:CLA (same ratio as present in LCNPs). Microtiter plates were incubated at 37°C for 18h and interpreted in accordance to the EUCAST BMD reading guide (version 5.0).

Molecular dynamic simulation of hexosomes

Simulation systems description

In paper II, to develop a model H_{II} system, we first created a bilayer with a PHY:FAR (90:10) ratio using the MemGen website.[99] The bilayer contained 100 lipids, 35 water molecules per lipid, and had an area of 65 Å² per lipid. This bilayer was then used to generate an inverted cylindrical micelle structure using the BUMPy toolkit by selecting only the inner leaflet.[100]Next, it was merged with a water cylinder created using Packmol, ensuring six water molecules per lipid (nw) in a triclinic box, processed using gmx trjconv.[101]

This resulted in a single H_{II} system unit, which served as the foundation for additional systems. The ratio between PHY and FAR was selected to mimic the realistic H_{II} system setup.[22] To create systems with varying hydration levels (nw ranging from 4 to 6), we randomly removed water molecules using a simple in-house Python script. This approach formed the basis for four different drug-loaded systems: two with CLA and two with VAN. In the clarithromycin-loaded systems, one system had three clarithromycin molecules inserted randomly, while the other had three clarithromycin molecules placed specifically in the lipid phase. Similarly, in the vancomycin-loaded systems, one system had three vancomycin molecules inserted randomly, whereas the other had three vancomycin molecules placed in the water phase. To maintain a final hydration level of nw = 5 after drug insertion, we performed random deletions of either lipids or water molecules.

All-atom molecular dynamics simulations. In paper II, all simulations were performed using Gromacs 2018 and 2021, employing the Charmm36 force field.[102,103] Molecular topologies for PHY, FAR, clarithromycin and non-standard amino acid residues of Vancomycin were parameterized either by analogy with existing Charmm36 force field parameters, or using CGenFF (v. 1.0.0).[104,105] The penalty values for PHY, and FAR were low (<5). The Pluronic F127 polymer chain was modelled using the charmm-GUI polymer builder module.[106] Pluronic F127 is a triblock copolymer composed of polyethylene oxide (PEO) and polypropylene oxide (PPO) in a PEO100-PPO65-PEO100 structure, where the subscript number represents the number of repeat units in the structure. Both PEO and PPO topologies were directly obtained from charmm-GUI server. Each system was energy minimized using the steepest descent algorithm for 10 000 steps, followed by equilibration of density and pressure for 100 ps. Final production runs were conducted for 500 ns for each system with a time step of 2-fs, employing periodic boundary conditions in all three directions. The system temperature was maintained at 30°C using the velocity rescale thermostat. Electrostatic interactions were calculated using the Particle Mesh Ewald method with short range electrostatic cut off at 1.2 nm, while van der Waals interactions were evaluated with a force-switch ranging between 0.8 and 1.2 nm.[107] Semi-isotropic pressure coupling was applied using the Parrinello−Rahman barostat (reference pressure = 1 bar), coupling time constant = 5 ps, and compressibility = $4.5e^{-5}$ bar^{-1}.[108]

Simulation analysis

In paper II, Structural parameters of H_{II} model systems were calculated following previous studies.[109,110] Order parameter was calculated by taking the absolute values of SCD, averaged over the last 100 ns, with the equation: $|S_{CD}| = \left|\frac{\langle 3\cos^2\theta - 1\rangle}{2}\right|$. This was only done for the backbone chain of PHY using gmx order function in Gromacs and plotted at all hydration levels and does not account for the four branching methyl and three hydroxy groups in the molecule.

Other structural parameters analyzed were the lattice plane distance or lattice parameter (dhex): $d_{hex} = \frac{\left(\sqrt{\frac{3}{2}}\right)X+Y}{2}$, where X and Y are the box dimensions of the system, the radius of the water cylinder $R_w = a\sqrt{\varphi_w\left(\frac{\sqrt{3}}{2\pi}\right)}$, and the area per lipid $APL = \frac{(\sqrt{3}\,\pi R_w V_l)}{(d_{hex}{}^2\varphi_l)}$.[109]

In order to calculate these structural parameters several variables of the systems needed to be known. First a box of 15,000 water molecules were simulated at 300K and the volume of a single water molecule was extracted in order to calculate the volume fractions of lipids $\left(\varphi_l = \frac{V_{lipids}}{V_{total}}\right)$ and water$(\varphi_w = 1 - \varphi_l)$ respectively, for the drug loading systems. Lastly, the lattice spacing a is equal to $\left(\frac{2}{\sqrt{3}}\right)d_{hex}$.

The number of contacts between different molecules were calculated using *gmx mindist* with a cut off distance of 0.5 nm and with using the option *-group yes*. In this option, a contact of an atom in another group with multiple atoms in the first group is counted as one contact.

Umbrella sampling simulations

In paper II, umbrella sampling (US) simulations were conducted to compute potential of mean force (PMF) profiles for drug molecules being pulled from the interior of the H_{II} system to the exterior excess water phase. A series of configurations were generated along the reaction coordinate, defined as the distance from the drug molecule's initial position to the bulk water phase in the x-direction (perpendicular to the cylinder). In total, 45 configurations, spaced 0.2 nm apart along this coordinate, were prepared. Each configuration served as a starting point for US simulations. Prior to the 12 ns production run, all configurations underwent energy minimization and equilibration. The weighted histogram analysis method (WHAM) implemented in Gromacs (*gmx wham*) was used to extract the PMF along the reaction coordinate from the US simulations.[111]

Cytotoxicity and cellular uptake of lipid nanoparticles

Cell culture

In paper III, human colorectal adenocarcinoma cell lines Caco-2 (originally obtained from the American Type Culture Collection, ATCC HTB-37™, Manassas, VA, USA), passage 95–105, were maintained in complete cell culture medium (Dulbecco's modified Eagle's medium, containing 10% (v/v) fetal bovine serum, and 1% (v/v) nonessential amino acids) at 37°C and 10% CO_2The cells used for all experiments were used within 10 passages after thawing. All cellular uptake and viability experiments were conducted under penicillin-streptomycin free complete medium, while trans-well permeability experiments were conducted under penicillin-streptomycin complete cell culture medium.

In vitro cytotoxicity assays

In paper III, Caco-2 cells (ATCC HTB-37™, passages 95 – 105) were seeded into black, clear-bottom 96-well plates (Corning®) at 5×10^4 cells per well in 300 µL complete DMEM (10 % FBS, 1 % penicillin–streptomycin, 1 % non-essential amino acids) and allowed to attach for 24 hrs at 37 °C and10% CO_2. Medium was then aspirated and replaced with 100 µL of lipid-nanoparticle dispersions diluted in the same medium to give final concentrations of 6.125 - 400 µM; each concentration was run in triplicate and every experiment was repeated independently in triplicates. After a further 24 h incubation, wells were washed twice with fresh medium to remove non-internalised particles. PrestoBlue® reagent (Thermo Fisher Scientific) was added directly to the wells at a 1:10 (v/v) dilution in culture medium (i.e., 30 µL reagent + 270 µL medium well^{-1}). Following the manufacturer’s recommended incubation (60 min, 37°C), fluorescence was recorded on a Spark multimode plate reader (Tecan, Australia; λ_{ex} 560 nm/λ_{em} 590 nm). Background fluorescence was subtracted using control wells that contained medium and reagent but no cells. Percentage viability was calculated relative to untreated controls, and data (mean ± SD) were analysed in GraphPad Prism 9.0 (GraphPad Software, USA).

Permeability experiments

In paper III, to measure *in vitro* apparent permeability, Caco-2 cells were Cells were seeded in triplicate into 12-well Transwell® inserts with polyester membranes (0.4 µm pore size, 1.12 cm^2 area, Corning Inc., Kennebunk, ME, USA) at a density of 1.5×10^5 cells per insert in 0.5 mL of culture medium in the apical chamber and 1.5 mL in the basolateral chamber for 21 days to ensure full monolayer differentiation and tight junction formation before permeability experiments. Prior to the experiment, the Transwell inserts were washed and equilibrated by transferring them into a pre-warmed HBSS washing plate followed by the addition of 0.5 mL of HBSS to the apical chamber, then incubated at 37 °C for 15 min on a shaker at 500 rpm. Samples (100 µL) were collected and 500 µL were disposed from the basolateral side at 15, 30, 60, 90, 120 min. After each sampling, 600 µL of fresh pre-warmed HBSS + 0.5% DMSO was added to the basolateral side to maintain volume. The apparent permeability coefficient (P_{app}) for VAN was calculated using equation below:[112,113]

$$P_{app} = \frac{dQ}{dt} \times \frac{1}{A \times C_0}$$

where, dQ/dt is the amount of compound change over time at steady state (µmol/s), A is the surface area of the monolayer (1.12 cm^2), C_0 is the initial concentration of the tested compound in the donor chamber (µmol/cm^3).[112,113] The rate dQ/dt as determined from the linear portion of the cumulative transport curve (based on concentrations measured at 15, 30, 60, 90 and 120 min). P_{app} were expressed in cm/s. Monolayers with $P_{app} > 1 \times 10^{-6}$ cm/s were considered to have compromised integrity and were excluded from further analysis.

Cell uptake of lipid nanoparticles by Caco-2 cells

In paper III, Caco-2 cells were seeded into 6-well plates (Corning® Falcon® Cell Culture Plate, Merck, Darmstadt, Germany) at a density of 1×10^6 cells per well in 1 mL of complete cell culture medium and incubated for 24 h at 37°C, 10% CO_2. On the following day, the cells were incubated with either hexosomes, cubosomes or liposomes (all labeled with R18) at 50 µM (total lipid) for 4 h. This experiment was performed at 37 °C and 4 °C to distinguish particle internalization from particle attachment on the cell surface (membrane trafficking is blocked at 4 °C).[80] For the assay at 4 °C, cells were kept at 4 °C for 2 h before treatment with nanoparticles. Cell uptake was quantified using flow cytometry (section below).

Cellular uptake of lipid nanoparticles by Caco-2 cells with endocytic inhibitors

In paper III, Caco-2 cells were seeded into 6-well plates (Corning® Falcon® Cell Culture Plate, Merck, Darmstadt, Germany) at a density of 1×10^6 cells per well in 1 mL of complete cell culture medium and incubated for 24 h at 37°C, 10% CO_2. To determine the dependence of different nanoparticles on specific endocytic pathways, dynasore and cytochalasin D were used as endocytosis inhibitors.[80,114] Before treatment, cells were washed two times with PBS (pH 7.4) to remove residual serum. Subsequently, 1 mL of either dynasore (80 μM), cytochalasin D (1 μM) or a combination of both in complete medium was added to the corresponding wells.[80,114,115] Cells were pre-treated with inhibitors for 1 h at 37°C, 10% CO2. After treating with inhibitors, 1 mL diluted R18-labelled nanoparticle dispersion was added to the same wells without removing the inhibitor solution, resulting in a final nanoparticle concentration of 50 μM. After the 4 h incubation with nanoparticles, cells were then trypsinized, added whole cell culture media, transfer to Eppendorf tube, and then centrifuged at 3500 rpm for 5 min, and resuspended by adding 1 mL LIVE/DEAD™ Viability/Cytotoxicity Kit (1μL/ml in PBS, Merck, Darmstadt, Germany) for 30 min on ice in dark room. After stanning, cells were washed with PBS three times, and resuspended in 1 mL of PBS and analyzed using flow cytometry (section below).

Flow Cytometry

In paper III, the Beckman Coulter Cytoflex LX (Beckman Coulter, USA) was used to quantify nanoparticles uptake. The cell population was identified in a FSC-A versus SSC-A plot, followed by gating for the living cells (excitation 405nm, emission 450/45), followed by single cell discrimination using FSC-H vs FSC-W and SSC-H vs SSC-A. To monitor internalized R18-labeled nanoparticles, identifiable by their fluorophore “rhodamine B 555”, a channel under the 561nm Laser (for excitation) was used, having the band pass filter of 585/42. We aimed to collect a minimum of 10.000 cells the singlet gate “siS” (SSC-H vs SSC-A), which was the last gate before the gating to monitor the nanoparticle uptake. Data analysis were performed using Cytexpert (2.6.0.105, Beckman Coulter).

3D printed tablet characterization

Preparation of gels for 3D printing

In paper IV, blank hexosome and VAN-loaded hexosome were prepared by previous protocol.[22] Different polymer compositions were tested by dispersing methyl cellulose (MC, A4C and/or A4M) and Ac-Di-Sol into the concentrated LCNPs, with all polymer amounts calculated based on the water content of the formulation. The final volume of each gel formulation was adjusted to maintain a consistent water phase to ensure comparability between batches. VAN-loaded LCNPs were prepared using the same protocol and collected in an identical manner. These VAN-LCNPs were directly used to prepare gels based on the optimized polymer composition identified during method development. The VAN-LCNPs were preheated at 70°C for 5 min in an oven (Termaks 10726, Fjärås, Sweden). MC was added gradually to the preheated dispersion (first MC A4C, then MC A4M), alternating with vortex mixing and reheating at 70°C (approximately 2–3 min per addition cycle). Ac-Di-Sol was subsequently incorporated using the method as for MC. After adding all polymers, the mixture was vortexed and placed on a shaker (type and company) at 37°C for around 10 min to achieve homogeneity. The gel formulation was then stored overnight at 4°C prior to 3D printing.

3D-printing of LCNP-containing gel

In paper IV, 3D-printing was performed using a Bio X 3D-printer (Cellink, Gothenburg, Sweden) equipped with a pneumatic printhead. A 3 mL syringe cartridge was filled with gel containing either blank LCNPs or VAN-LCNPs, and a printing nozzle with an inner diameter of 0.41 mm was mounted. Printing parameters such as printing speed and pressure were individually adjusted based on gel composition to ensure consistent deposition. The applied pressures ranged from 140 to 200 kPa, with printing speeds between 2 and 3 mm/sec (Table S4). A cylindrical 3D model with a diameter of 10 mm, a height of 3 mm, and an infill density of 100% was used. Printing was conducted at room temperature directly onto plastic weighing dishes. Standard size of tablets was selected to be 10 x 3 mm (diameter x height), and alternating sizes, such as 12 x 3 mm, 8 x 3 mm, 5 x 3 mm, 3 x 3 mm and 10 x 2 mm were printed for dose accuracy studies. After printing, the tablets were dried in a vacuum oven (Vacutherm, Thermo Fisher Scientific, Massachusetts, USA) at 400 mbar and 40 °C for approximately 24 h. Drying was considered complete when the deviation between the weight loss and theoretical amount of water in the tablets was less than 10%.

Rheology

In paper IV, rheological measurements of the gel were performed after overnight storage at 4°C using an ARES-G2 rheometer (TA Instruments, New Castle, DE, USA). All analyses were conducted at 25°C with a stainless-steel parallel-plate geometry (diameter = 8 mm) and a flat plate (diameter = 60 mm), with a set gap of 0.5 mm. The gel sample was applied onto the flat plate using a plastic spatula, after which the geometry was lowered to the defined gap at a rate of 0.1 mm/s. Excess gel was removed, and the sample was equilibrated at the set temperature for 3 min before each measurement. The range of shear rates for flow sweeps was 0.001 – 500 s^{-1} with five data points per decade and a steady state sensing including three consecutive measurements, a sample period of 10s, 5% tolerance and a maximum equilibrium time of 120s. To determine yield strain and linear viscoelastic (LVE) range, amplitude sweeps were performed. The oscillation strain was increased from 0.01% to 500% with ten measurements per decade. Angular frequency was kept constant at 1.0 Hz. The yield point was assessed by fitting two lines to the G' (storage modulus) graph using a linear regression model to the log-log transformed data. This yields the following formula for a linear equation:

$$Y = \log_{10} G' = m \cdot \log_{10} \gamma + \log_{10} n \ = mX + n$$

where γ is the shear strain, m is the slope and n is the y-intersect of the linear equation. The first regression was performed at the plateau of G' at low strains between 0.01% and 0.25%. The second line was fitted to the region of linearly declining G' between 10% and 50%. The crossover point of these lines was taken as the yield point. For the purpose of this study, the end of the LVE range was defined to be the strain at which the actual G' deviated from the G' according to the linear fit in the plateau by more than 5%. Based on the amplitude sweep, the strain for the frequency sweep was set to 0.05%, while the frequency range was between 0.01 and 100 Hz, again with ten points per decade. The measurements were performed from high to low frequencies to minimize inertia effects. Finally, gel recovery was assessed under vibratory conditions for cycles of different strain. First, 0.05% shear strain was applied for 300 s in cycle I, then 100% shear strain was applied for 150 s in cycle II. Cycle III used the same parameters as cycle I). One measurement was taken per second in all three cycles. The amount of elastic properties recovered after application of shear strain on the gel were calculated using:

$$Recovery\ [\%] = \frac{Average\ G'\ of\ cycle\ III)}{Average\ G'\ of\ tcycle\ I)} \cdot 100\%$$

Tablet dimensions and uniformity of mass

In paper IV, diameter and thickness of the 3D-printed tablets containing blank LCNPs were measured with a traceable digital caliper (VWR, Stockholm, Sweden). The weight of tablets (on at least 5 tablets per formulation) was measured directly after 3D-printing (wet weight) and after drying (dry weight) using an analytical balance (Sartorius Entris 224i-1s, Goettingen, Germany).[116] All weight measurements were completed in on at least 5 tablets. Mass uniformity of the 3D-printed tablets was assessed according to 2.9.5. (Ph. Eur., 11th edition).

In vitro disintegration of 3D-printed tablets

In paper IV, the *in vitro* disintegration behavior of tablets containing blank LCNPs (n = 6) was evaluated using a basket-rack assembly with discs (Pharma Test PTZ-S, Hainburg, Germany).[117] Each tablet was placed individually into one of the six baskets of the apparatus, which was immersed in 650 mL distilled water maintained at 37.0 ± 2.0 °C. The basket was lifted vertically at 30 cycles/min, and tablet disintegration time was automatically recorded.

Uniformity of content and dose accuracy

In paper IV, to evaluate the uniformity of drug content and accuracy, a total of 10 tablets containing VAN-LCNPs (10 x 3 mm) were randomly selected out of a batch containing 15 tablets. Each tablet was dissolved in 1.5 mL acetonitrile, followed by centrifugation at 14,000 × *g* for 10 min at 37°C. Acetonitrile was removed under a nitrogen stream, and the residue was re-dissolved in water and diluted with water (add dilution). Then 100 µL of the supernatant was transferred to HPLC-vials for HPLC-UV analysis as described in section above. In total, tablets in 5 different sizes were printed: 10 × 3 mm, 10 × 2 mm, 8 × 3 mm, 5 × 3 mm, and 3 × 3 mm. All tablets were weighed after drying, and drug content was quantified using the same HPLC-UV method described before.

Results and discussion

Engineering LCNPs with defined internal architectures for oral antibiotic delivery

Phase behavior and structural characterization

For our first goal towards LCNP formulations for oral delivery of antibiotics, we needed to engineer LCNPs that could efficiently load both hydrophilic (VAN) and hydrophobic (CLA) antibiotics, thereby facilitating their combination therapy. To do this, we first prepared cubosome and hexosome LCNPs, verified their internal architectures and measured their loading capacity. To compare the performance of internal cubic versus hexagonal phase, we utilized cubosomes based on PHY and developed novel hexosomal particles utilizing PHY in combination with the lipids TOC and FAR which, due to their stable chemical structure, are less susceptible to hydrolytic degradation by lipases present in the GIT.[22]

The phase diagram of LCNPs systems showed that PHY alone yielded cubic phases, the addition of TOC and FAR led to formation of inverse hexagonal phase (H_{II}) (Fig.10A-C).
Their liquid crystal phase maintained across a temperature range of 10-50°C with characteristic Bragg peaks at 1, √3, √4, with lattice parameters decreasing from 24.55 to 21.95 Å (PHY/TOC) and 21.50 to 20.04 Å (PHY/FAR) between 10-50°C (figure 10). Their internal structure confirmed by cryo-TEM to possess distinct cubic and hexagonal architectures with characteristic parallel striations. (figure 11A, E, I).

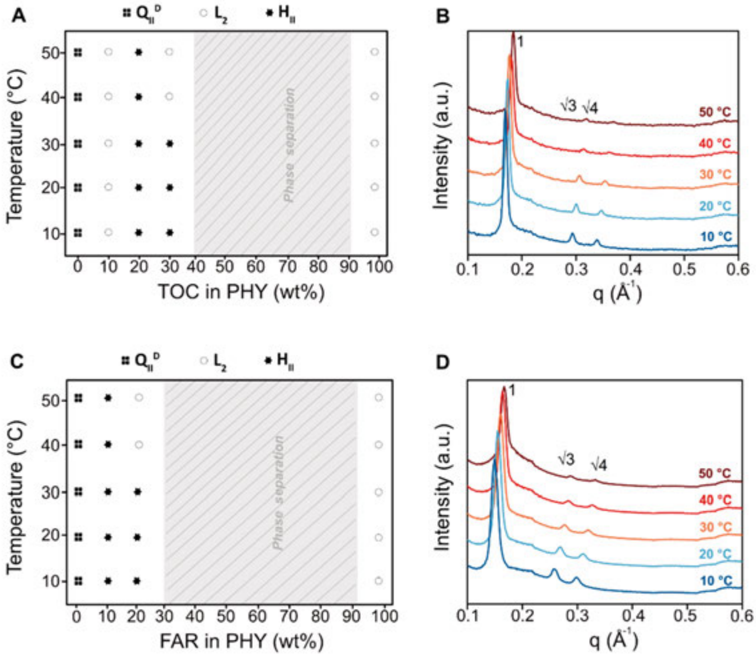

Figure 10. SAXS characterization of LCNPs composed of either PHY/TOC and PHY/FAR lipid mixtures. **(A)** Phase diagram obtained by SAXS measurements of PHY/TOC-based LCNPs at different weight ratios (0-100%) and temperatures (10-50°C). **(B)** Representative 1D SAXS patterns of intensity against the scattering vector q for 20 wt% TOC in PHY as a function of temperature. **(C)** Phase diagram obtained by SAXS measurements of PHY/FAR-based LCNPs at different weight ratios (0-100%) and temperatures (10-50°C). **(D)** Representative 1D SAXS patterns of intensity against the scattering vector q for 10 wt% FAR in PHY as a function of temperature. Phase separation indicates samples that visibly separated into distinct phases before SAXS analysis, preventing analysis due to lack of homogeneity. Q_{II}^{D} (Pn3m bicontinuous cubic phase); L_2 (inverse micellar); H_{II} (inverse hexagonal).

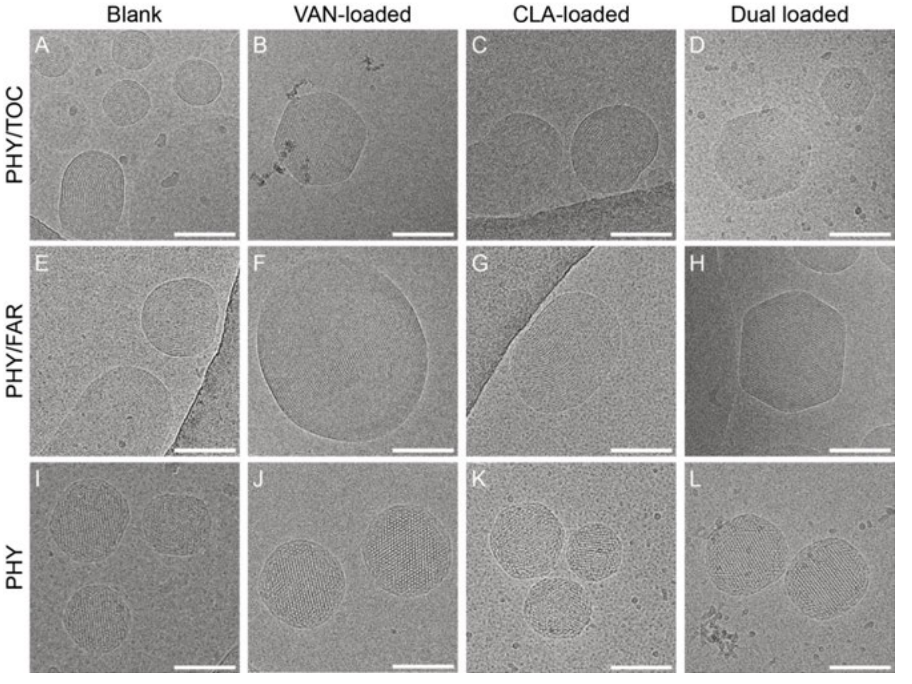

Figure 11. Morphological characterization of LCNPs. **(A, E, I)** Representative cryo-TEM images of blank LCNPs based on either PHY/TOC hexosomes, PHY/FAR hexosomes or PHY cubosomes. **(B, F, J)** Representative cryo-TEM images of single loaded with either VAN or **(C, G, K)** CLA and **(D, H, L)** dual loaded (VAN+CLA) LCNPs. Scale bars, 100 nm.

Drug loading and compartmentalization dynamics

In our initial effort to produce nanoparticle formulations suitable for antibiotic combination therapy, we chose a co-administration and dual-loaded strategy. Co-administration allows the formulation of each drug to be individually optimized for each drug, ensuring that each component is loaded in its most effective and stable form.

Dual-loaded approach allow both CLA and VAN together inserted into one nanoparticle. To assess the loading capacity of the nanoparticles, we formulated each LCNP containing VAN or CLA individually at various concentrations, ranging from 1 to 5 mol%. VAN was expected to preferentially partition into the water channels of the LCNP, and CLA into the hydrophobic lipid leaflets.

Encapsulation efficiencies reached 84-90% for both VAN and CLA in co-administered systems, 69-72% in dual-loaded LCNPs. To confirm the drug entrapment, DOSY-NMR revealed CLA diffusion coefficients decreased 10-fold upon encapsulation (5.99×10^{-10} to 4.34×10^{-11} m^2/s) after loading with LCNPs, confirming lipid matrix confinement. VAN maintained similar coefficients ($3.05\text{-}4.21 \times 10^{-10}$ m^2/s) due to self-assembly into micelles above its CMC (0.72 mg/mL).

Gastrointestinal stability and *in vitro* release

The LCNPs were fabricated with lipids chosen for their chemical stability. Here, we proposed they would be less susceptible to digestion in the GI environment, with the aim of conserving the NP internal nanostructures until they reach the small intestine for absorption.

LCNPs being designed for oral administration therefore require an assessment of their resistance to degradation by intestinal enzymes in order to optimize cargo protection.[75,118] Lipolysis experiments to measure the capacity of our LCNPs to endure this environment were performed using a standardized in vitro setup (Fig. 12A). Here we specifically focused on evaluating their susceptibility to digestion by pancreatic enzymes, such as lipases, which cleave ester bonds in lipids to release FAs.

LCNPs demonstrated exceptional enzymatic resistance with <2.6% lipolysis after 60 min pancreatic lipase exposure versus 75.1% for GMO controls (Fig. 12B). To thoroughly evaluate the drug release dynamics of the studied LCNPs, we employed pressure ultrafiltration followed by reverse phase HPLC to offer insights into the maximal achievable drug release. Co-administered formulations retained >80% of both antibiotics during lipolysis, while dual-loaded systems released 32-40% (Fig. 12C and D).

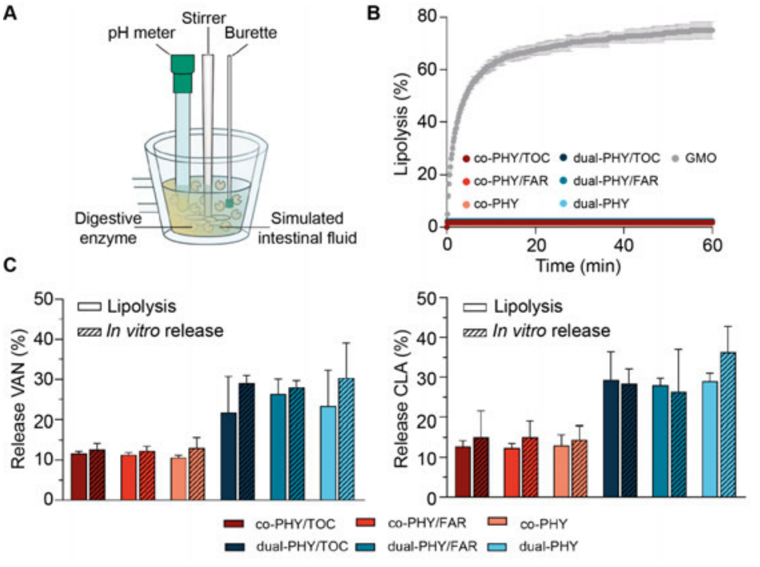

Figure 12. In vitro lipolysis of LCNPs and antibiotic release. **(A)** Standardized setup for in vitro lipolysis assays using pH stat titration. **(B)** The percentage of lipolysis occurring over time with pancreatic lipase for co-administered (50:50 VAN:CLA loaded LCNPs) and dual loaded (VAN+CLA) LCNPs based on PHY/TOC hexosomes, PHY/FAR hexosomes or PHY cubosomes. GMO-based cubosomes served as control. **(C)** Comparison of release of VAN (left panel) and CLA (right panel) during in vitro release and lipolysis of antibiotic-loaded LCNPs. Lipolysis data was retrieved from sampling during assay shown in A-B. Data is shown as mean ± SD, n = 3.

The efficiency of oral antibiotic therapies to treat systemic infections is greatly challenged by poor water solubility and low permeability across the intestinal mucosal barrier. High drug doses are often required to establish an effective concentration gradient for absorption. However, excessive exposure to antibiotics can disrupt the gut microbiota, leading to adverse reactions.[3] To address these challenges, LCNPs could be used to deliver the drug to the site of absorption in the GIT with minimal premature leakage, thereby mitigating collateral damage to our commensal gut microbes.

In assessing the protective capability of LCNPs against intestinal bacteria, Gram-negative *E. coli* and Gram-positive *E. faecalis* were selected as representative members of the human microbiome.[119] They are both found in high abundance in the human gut and can be cultivated and manipulated without using anaerobic conditions.[119,120] Extensive research on the ATCC strains used in this study provides a well-established background of their behavior under antibiotic exposure, allowing for accurate interpretation of experimental results. Bacterial growth inhibition assays were conducted to study the efficacy of antibiotic-loaded LCNPs (single, co-administered and dual), using unformulated antibiotics as controls (Fig.13).

To investigate whether encapsulation of antibiotics into carrier systems would protect our two representative bacterial strains, MIC assays were initially performed using LCNPs loaded with a single antibiotic at 1 mol%. Against *E. coli*, all VAN/CLA-loaded LCNP types were protective, returning MIC values above the assay detection limit (Fig. 13A). This protective effect was less pronounced against the Gram-positive *E. faecalis*. VAN-loaded PHY/TOC and PHY/FAR offered an eight-fold increase in MIC values compared to the control (16 vs 2 μg/mL), and FAR loaded particles were less effective (MIC: 8 μg/mL) (Fig. 13B).

Next, we assessed the impact of co-administered and dual-loaded LCNPs, specifically designed for antibiotic combination therapy, on bacterial growth inhibition. As controls, we first determined the MIC values of a VAN/CLA mixture (1:1 mol% ratio, as present in LCNPs) against *E. coli* (32 μg/mL) and *E. faecalis* (1 μg/mL) (Fig. 13C-D). Co-administering a mixture of VAN- and CLA-loaded LCNPs yielded formulations with no detected MIC values against *E. coli* (MICs: >1024 μg/mL, Fig. 13C). Dual-loaded nanoparticles also offered protective effects (MICs: 512 μg/mL, Fig. 13C). The increased susceptibility of *E. coli* towards the dual-loaded systems is consistent with our stability and release data (Fig. 12C), which showed that, in general, dual-loaded LCNPs released more antibiotic into the surroundings. Despite this variation between particle loading strategies, MIC values were significantly higher than non-formulated controls, verifying our proof of concept. Against *E. faecalis*, both co- and dual-loaded systems returned MIC values above the control of 1 μg/mL; 8 μg/mL for all formulations with the exception of co-FAR/PHY (16 μg/mL) (Fig. 13D).

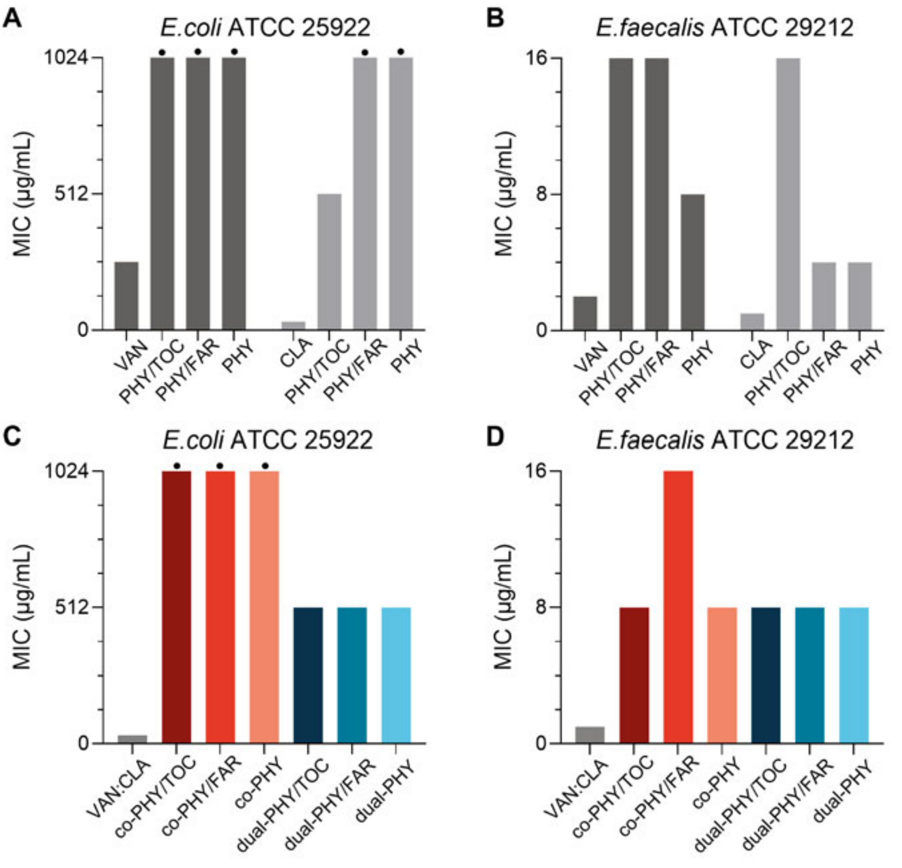

Figure 13. Effect of antibiotic loaded LCNPs on growth of two representatives of commensal gut bacteria. (A, B) Free antibiotics and LCNPs loaded with 1 mol% of either VAN or CLA were tested against isolated strains of (A) *E. coli* and (B) *E. faecalis* using a broth dilution assay. (C, D) LCNPs encapsulating VAN and CLA in co-administered (co-) and dual-loaded (dual-) approach were tested against isolated strains of (C) *E. coli* and (D) *E. faecalis* using a broth dilution assay. Bars marked with • had MIC values above the limit of detection.

For both strains, the MIC values of the combinations reflect the MIC of CLA alone, indicating a lack of detectable synergy between VAN and CLA against both *E. coli* and *E. faecalis*. Previously reported synergy for the VAN +CLA combination was observed against *Mycobacterium abscessus*[121], a Gram-positive bacterium more susceptible to VAN than Gram-negative bacteria due to its ability to penetrate the outer membrane. Similarly, in vitro activity of a VAN and CLA combination has been demonstrated against Gram-positive *Staphylococcus aureus*.[122] The lack of synergy against Gram-positive *E. faecalis* may be due to the tested 1:1 mol% ratio not being optimal for achieving synergy.

Molecular mechanisms governing drug-LCNP interactions

Structural parameters and hydration effects

We first assessed the structural stability of the PHY:FAR (90:10) H_{II} system by simulating a single water channel surrounded by lipids at varying water-to-lipid ratios. MD simulations H_{II} systems revealed linear correlations between hydration (number of water-to-lipid molecules (n_w) = 4-6)) and structural parameters: lattice parameter (41.1-46 Å), water channel radius (10.2-13.5 Å), and area per lipid (23.1-25.1 Å^2). Systems equilibrated within 300-350 ns, maintaining hexagonal packing across all hydration levels, though lower hydration induced pronounced channel curvature deviating from ideal cylindrical geometry. To further evaluate structural integrity, we analyzed simulation snapshots at the end of each run. As illustrated in Figure 14, hexagonal packing was preserved across all hydration levels. However, at nw = 4, the water channel exhibited pronounced curvature along the cylinder axis, deviating from an ideal cylindrical shape. With increasing hydration, the water cylinder expanded and adopted a more stable, cylindrical geometry. This behavior mirrors previous findings in DOPE-POPE H_{II} systems, where higher hydration levels reduced undulations and promoted cylindrical symmetry.[109]

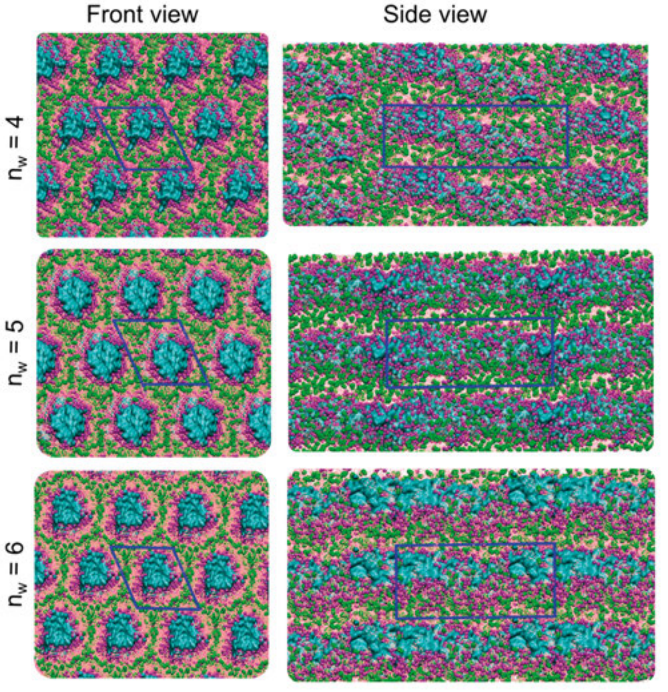

Figure 14. Representative simulation snapshots of the PHY:FAR (90:10) H_{II} systems at different hydration level. Color representation: The magenta and green beads represent the lipid headgroup oxygen and the last carbon atoms in the tail, respectively. The pink dots illustrate the remaining parts of the lipid tails. Water is shown as cyan surface. The blue lines indicate the boundaries of the simulated system.

Drug localization and interface dynamics

Following confirmation of the structural stability of the PHY:FAR H_{II} system, we next examined how drug molecules interact with different constituents that are part of the internal environment of the H_{II} phase. To this end, we conducted simulations using four distinct systems involving two drug compounds: CLA and VAN. Each system employed the same H_{II} model, consisting of a single water cylinder surrounded by PHY:FAR (90:10) at a water-to-lipid ratio of n_w = 5. CLA was incorporated into two systems: one where it was randomly inserted and another where it was specifically placed within the lipid phase (Figure 15A and C). Similarly, VAN was introduced either randomly or directly into the water phase (Figure 15B and D).

To quantify drug - matrix interactions, we calculated the number of contacts between each drug and the lipid or water components. For CLA, random insertion led to a rapid increase in lipid contact - from approximately 0.55 to

0.75 - within the first few nanoseconds, after which it stabilized around 0.75 (Fig. 15C). When CLA was initially placed in the lipid phase, the initial contact was higher (~ 0.9), but both systems eventually exhibited similar contact profiles, indicating a strong preference for the lipid environment regardless of initial placement. For VAN, the initial drug - water contact was approximately 0.4 for random insertion and 0.6 when placed directly in the water phase. Over time, both systems converged to a stable drug-water contact of ~ 0.5, with a similar proportion of drug-lipid contacts. This suggests that VAN equilibrated at the water-lipid interface, interacting with both environments. VAN is a branched, tricyclic glycosylated nonribosomal peptide composed of both hydrophobic and hydrophilic residues. Further residue-level analysis revealed that specific residues, such as residues 1, 2, 4, and 6 - preferentially interacted with the lipid phase, supporting its interfacial localization (see Paper II, S3).

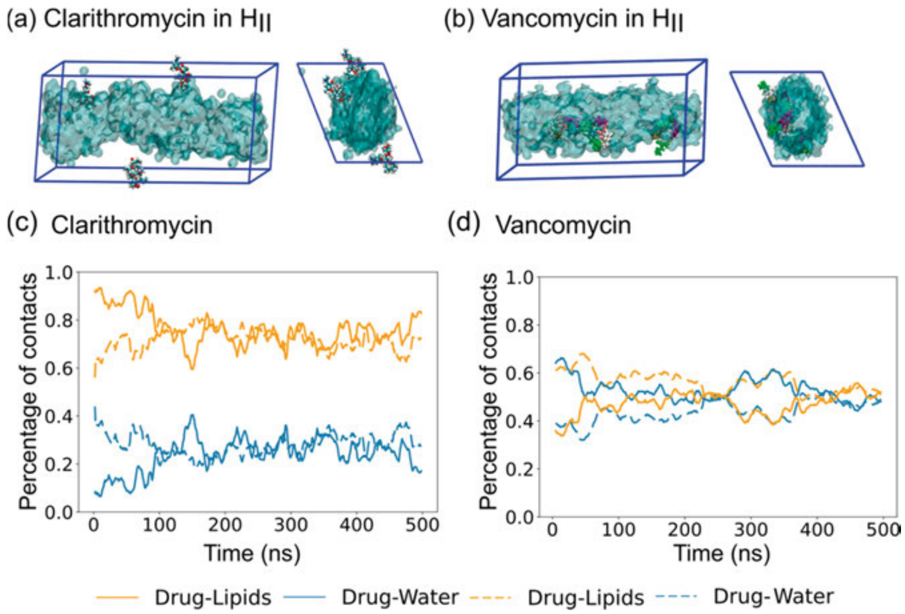

Figure 15. Interaction between clarithromycin and vancomycin with the PHY:FAR (90:10) H_{II} system constituents. (**A**) and (**B**) show representative snapshots of the HII system loaded with clarithromycin and vancomycin, respectively, from a side and front view. (**C**) and (**D**) illustrate the fraction of contacts between clarithromycin and vancomycin and the H_{II} constituents, respectively. In (**C**) and (**D**), dashed lines represent cases where the drugs were inserted randomly, while solid lines indicate simulations where drugs were inserted specifically into the lipid phase or water phase of the H_{II} system. The sum of drug-lipid and drug-water contacts at any given time equals 1.

Overall, these simulations indicated that clarithromycin, due to its high lipophilicity, predominantly associates with the lipid bilayer. In contrast, vancomycin, with its amphiphilic character, tends to localize at the water–lipid interface, forming stable interactions with both phases. These findings provide molecular–level insight into how drug physicochemical properties influence their distribution and retention within H_{II} phase systems.

LCNP-epithelial barrier interactions and permeation mechanisms

Energy-independent cellular internalization

Understanding how the internal nanostructure of lipid-based nanocarriers affects cellular uptake is critical for optimizing oral drug delivery systems. To investigate this, we compared the uptake of various lipid nanoparticles with different internal structures in an intestinal epithelial model. Flow cytometry was used to quantify the extent of nanoparticle uptake by Caco-2 cells. Cells were exposed to PHY/TOC-hexosomes, PHY/FAR-hexosomes, PHY-cubosomes, and DOPC liposomes under metabolically active (37°C) and energy-depleted (4°C) conditions (Fig. 16A and 16B).

Interestingly, temperature restriction (4°C) reduced all uptake >80%, confirming membrane fluidity requirements (Fig 16B). At 4°C, the cell membrane is no longer a fluidic lipid instead approaching to the gel phase,[123] their lateral lipid diffusion coefficient drops by one to two orders of magnitude, membrane viscosity and bending rigidity rise, and surface tension climbs,[124] together imposing a high energetic barrier that stalls the transition from a hemifusion stalk to an open fusion pore.[123] Therefore, even curvature-promoting nanoparticles face restricted internalization at this point. However, PHY-cubosomes still exhibited a low but detectable residual signal at 4°C, likely reflecting surface binding or limited direct phase-through interactions rather than true internalization.

To better understand the cellular internalization routes utilized by lipid cubic and hexagonal nanoparticles (LCNPs) to enter intestinal epithelial cells, we investigated key endocytic pathways using pharmacological inhibitors. Based on this molecular landscape, we focused on two major pathways: dynamin-dependent endocytosis and macropinocytosis. These were selectively inhibited using dynasore (80 µM), a non-competitive inhibitor of dynamin GTPase activity, and cytochalasin D (Cyto D, 1 µM), which disrupts F-actin polymerization to block macropinocytic ruffling. Applied together (Cyto D + dynasore), these agents abrogate the two principal ATP-dependent uptake routes operative in Caco-2 cells.

Taken together, PHY/TOC-hexosomes (10.1 ± 7.2%), PHY/FAR-hexosomes (5.6 ± 6.6%), and PHY-cubosomes (2.7 ± 1.8%) are primarily internalized through non-endocytic, energy-independent mechanisms, whereas DOPC liposomes rely heavily on classical endocytosis, with over 60% of uptake attributed to dynamin- and actin-dependent processes (Fig. 16C, D and E). Pharmacological dissection using dynasore and cytochalasin D demonstrated LCNPs maintained >90% uptake under dual inhibition while liposomal uptake decreased to 10%, confirming non-endocytic, energy-independent internalization of LCNPs driven by membrane curvature.

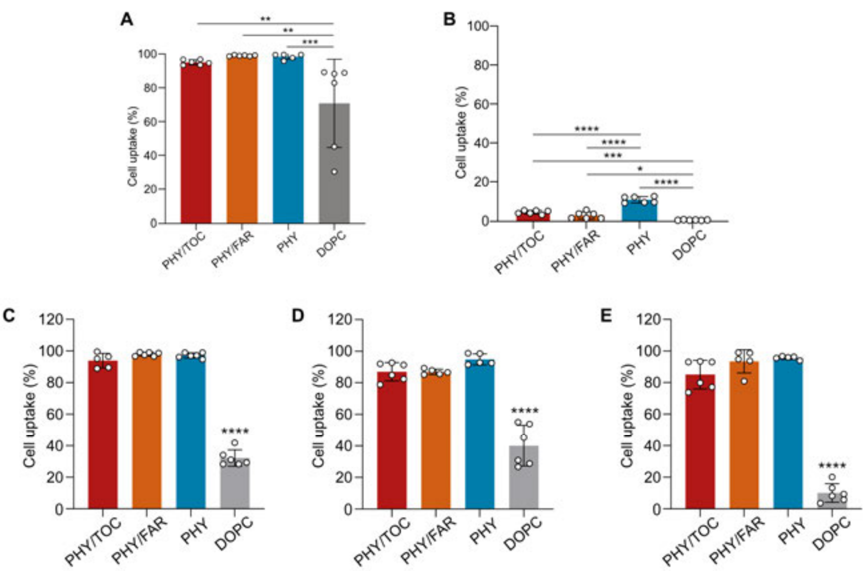

Figure 16. Internalization of R18-labelled LCNPs by Caco-2 cells as intestinal cell model. (**A**) Uptake efficiency at 37°C expressed as the percentage of R18-positive events relative to the uninhibited control population. (**B**) Uptake efficiency at 4°C expressed as the percentage of R18-positive events relative to the uninhibited control population. (**C**) Uptake after blocking dynamin-dependent routes (dynasore). (**D**) Uptake after blocking macropinocytosis (cytochalasin D) (**E**). Both dynamin-dependent endocytosis and macropinocytosis were inhibited. Bars are normalized to the corresponding uninhibited nanoparticle control (corresponding to 100%). Duplicates (n = 2). Statistical analysis was performed by one-way ANOVA with Tukey's post-hoc test: * $p \leqslant 0.05$, ** $p \leqslant 0.01$, *** $p \leqslant 0.001$, **** $p \leqslant 0.0001$.

Similar observation in line with previous study that using phytantriol/mannide monooleate-based hexosome show energy independent pathway,[80] together with Yap et al, showed that CME-independent pathway by using GMO-cubosome/hexosome for Chinese Hamster Ovarian (CHO) cells.[125] It should be noted, however, that not all studies converge on CME-independence: GMO-derived cubosomes were shown to be substantially dynamin-dependent in HepG2 hepatoma cells,[84] implying that the preferred entry route can vary with lipid composition, particle architecture, and the endocytic repertoire of the target cellEnhanced transepithelial transport

Having established safe concentration range for each LCNP formulation and its potential cell internalization, we next assessed their ability to enhance the transepithelial transport of VAN across intestinal epithelium. Due to its large size and hydrophilicity, free VAN is poorly absorbed when administered orally, making it an ideal model compound for evaluating the permeability-enhancing potential of lipid nanoparticles.[96,126] Using Caco-2 monolayers as a well-established in vitro model of the intestinal barrier,[113,127,128] we compared the transport efficiency of VAN encapsulated in hexosomes, cubosomes, and liposomes, relative to the unencapsulated drug.

VAN permeability across Caco-2 monolayers increased 13-fold when delivered via PHY cubosomes ($P_{app} = 6.0 \times 10^{-5}$ cm/s) compared to free drug (0.40×10^{-5} cm/s) (Fig.17B). Hexosomes achieved intermediate enhancement ($3.1\text{-}4.2 \times 10^{-5}$ cm/s) while DOPC liposomes showed minimal improvement (1.9×10^{-5} cm/s) over VAN alone (add Papp) (Fig.17B). The permeability ranking (PHY > PHY/TOC > PHY/FAR > DOPC >> free VAN) correlated with cellular uptake patterns, validating structure-function relationships between internal architecture and transport efficiency.

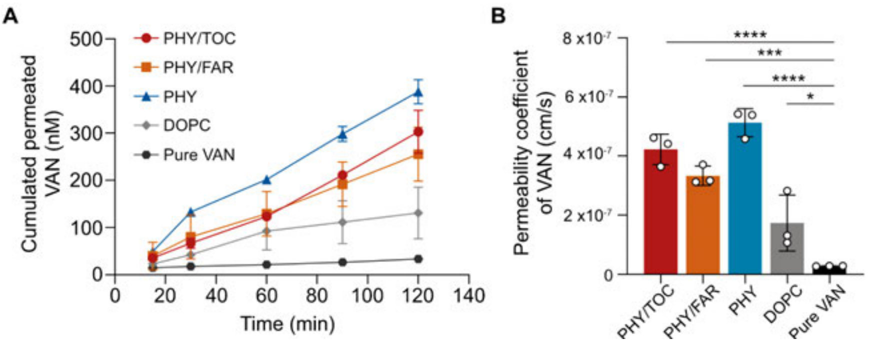

Figure 17. Permeability enhancement of VAN across Caco-2 cell monolayers by different LCNP formulations. (**A**) Cumulative amount of VAN transported to the basolateral compartment over 120 min for different formulations: PHY/TOC hexosomes, PHY/FAR hexosomes, PHY cubosomes, and DOPC liposomes. Free VAN served as the control. (**B**) Apparent permeability coefficients (P_{app}) of VAN after 120 min, corresponding to the formulations shown in (A). Statistical analysis was performed using one-way ANOVA with Tukey's post-hoc test; significant differences versus the free VAN control are indicated as $*p < 0.05$, $***p < 0.001$, and $****p < 0.0001$. All data are presented as mean ± SD from n = 2 replicates.

This correlation between cellular uptake and permeability suggests that the transport mechanisms established in undifferentiated cells may partially translate to differentiated monolayers, though the extent of enhancement may be modulated by the distinct membrane properties.

Translation to personalized solid dosage forms

SSE 3D printing optimization

To identify LCNPs suitable for 3D printing applications, we focused on PHY/TOC-based hexosomes due to their proven ability to self-assemble into stable nanostructures. In our previous studies (Paper I, S2A), PHY/TOC hexosomes maintained an internal hexagonal (H_{II}) phase structure with VAN concentrations up to 5 mol%.[22] Hence, we selected a 5 mol% VAN concentration for loading in our current LCNPs.

3D-printing of the prepared gels was performed using semi-solid extrusion (SSE), with printing parameters optimized for each individual gel, all of which were successfully printable (Paper IV, Table S4). Gels were prepared by addition of polymers either alone or in combination (MC A4C, MC A4M, Ac-Di-Sol) to the LCNP dispersion at 70°C. The consistency of the gel did not change visibly during the addition of MC in the hot dispersions. The addition of Ac-Di-Sol (Formulations 3-7) increased the gel viscosity already in the hot state, making the gel not flowable when tilting the container. Mixing was only achieved by vertexing in this state. For Formulations 5-7, the amount of Ac-Di-Sol that could be incorporated was assessed visually by the addition of Ac-Di-Sol until sufficient mixing could just be ensured.

A representative tablet printed from formulation 7 is shown in Fig. 18D, where the term "wet tablet" refers to its appearance immediately after the printing process. All formulations produced tablets with consistent wet masses (~ 200 mg, Fig. 18B). Following 3D-printing, the tablets were dried in vacuum at 40°C overnight to yield solid tablets (Fig. 18D, “dry tablet”). Tablet mass decreased significantly (to ~ 65-72 mg) upon drying (Fig. 18B-D), indicating substantial water loss.[129] The diameter of the 3D-model used to print tablets was 10 mm, while in the dried state the tablet diameter ranged from 6.9 to 7.5 mm. Tablets with higher overall polymer content (13% - 16.2%) in general had a larger diameter (Paper IV, Table S5).

To evaluate the performance of the 3D-printed tablets for LCNP release, their disintegration behavior was systematically assessed under various formulation and printing conditions. Tablet disintegration was tested using water as the disintegration medium. This step is critical for LCNP release, as the active pharmaceutical ingredient (API) remains trapped within the matrix unless the tablet fully disintegrates. The mean disintegration times of tablets with different compositions are presented in Fig. 17B. In general, a higher content of the disintegrate Ac-Di-Sol resulted in faster disintegration (e.g., Formulation 4-6). Disintegration times showed relatively high standard deviations (Fig. 18B). In some cases, the fastest disintegration for an individual tablet was nearly half of that of the slowest tablet within the same formulation. Notably, all tablets of Formulation 7 disintegrated within 32 min, with a mean disintegration time of 24 min. Due to its favourable disintegration profile, this formulation was selected for further characterization. Infill density also influenced disintegration time, as shown in Fig 18B. This was evaluated using Formulation 1. Tablets with 100% infill density disintegrated the slowest, while those with 25% infill density showed the fastest disintegration times. These low-density tablets successfully passed the disintegration test according to Ph. Eur. standards. Seven gel formulations were systematically evaluated, with Formulation 7 (8.4% Ac-Di-Sol, 4.2% MC A4C, 3.6% MC A4M) providing optimal rheological properties. Printing parameters ranged 140-200 kPa pressure at 2-3 mm/s speeds, producing tablets with consistent wet masses (~200 mg) that dried to around 65-72 mg.

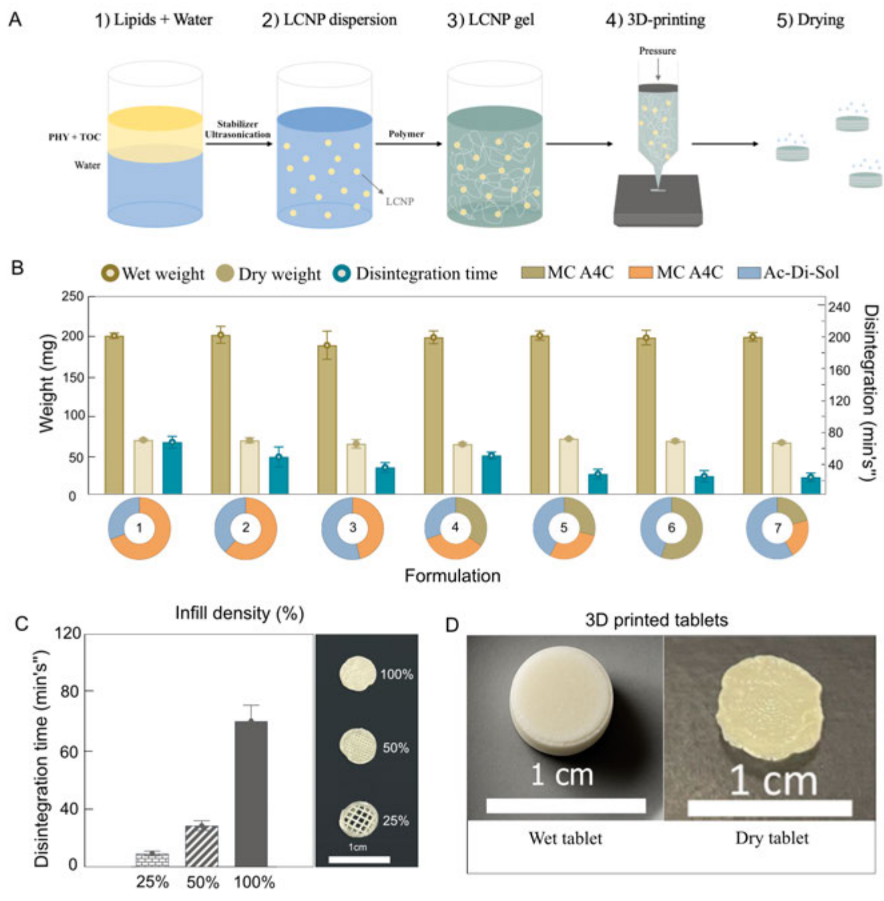

Figure 18. Gel optimization and production of 3D-printed tablets containing blank LCNPs. (**A**) Graphical overview illustrating the preparation and 3D-printing process of LCNP-based tablets. (1) Lipid components (PHY and TOC at a 4:1 ratio, total 20% w/w) mixed with water. (2) Formation of LCNP dispersion stabilized with Pluronic F127 via ultrasonication. (3) Polymer addition to achieve optimal gel consistency suitable for printing. (4) Semi-solid extrusion 3D-printing of LCNP-based gels. (5) Vacuum drying of printed tablets. (**B**) Physical characterization of LCNP tablets printed from seven distinct formulations with varying polymer compositions. Wet weights (green), dry weights (yellow), and disintegration times (blue) are shown for each formulation. The polymer compositions include MC A4C (green), MC A4M (orange), and Ac-Di-Sol (purple). Round dots represent the mean of each parameter, error bars represent standard deviation ($n \geqslant 5$). (**C**) Correlation between infill density (25%, 50%, and 100%) and corresponding disintegration times of dried 3D-printed tablets (left). Representative images of tablets at each infill density are shown (right). Error bars represent standard deviation ($n \geqslant 5$). (**D**) Photographs of a representative tablet before drying (wet) and after drying (dry). Scale bars represent 1 cm.

Structural integrity through processing and pharmaceutical quality attributes

To confirm LCNPs' integrity after rehydration of the tablet, SAXS and Cryo-TEM data are used. SAXS confirmed H_{II} phase preservation during gel formation and printing (lattice parameter around 44.9 Å) (Fig.19A). While dried tablets lost characteristic peaks, rehydration restored the hexagonal structure with slight lattice expansion (45.9 Å) and water channel enlargement (1.79 to 1.89 nm) (Fig. 18B). Cryo-TEM verified complete structural recovery without protective excipients, demonstrating intrinsic LCNP stability (Fig. 19C).

There are currently no specific regulatory guidelines dedicated to 3D-printed tablets with personalized dosages. In this proof-of-concept study, we therefore applied the conventional pharmacopoeial standards European Pharmacopoeia (Ph. Eur., 11th edition, sections 2.9.5 and 2.9.6) for oral tablets to evaluate both drug content and dose accuracy. The aim was to assess the critical quality attributes of LCNP-based tablets manufactured by SSE 3D printing. In our case, VAN-loaded LCNP tablets were printed using the optimized lead formulation (Formulation 7). All tablets (10×3 mm) fulfilled the pharmacopoeial criteria for mass uniformity (<7.5% deviation) (Fig.18E). However, two tablets exhibited drug content outside the 85–115% acceptance range (−16.1% and −16.3%), indicating that the drug content uniformity did not fully comply with Ph. Eur. Requirements (Fig.19F). To further demonstrate the flexibility of this approach in tailoring personalized dosages, we also printed tablets of varying sizes (Fig.19D), which showed a strong size–dose correlation ($R^2 = 0.93$ between drug content and weight; see Paper IV, Figure 5D).

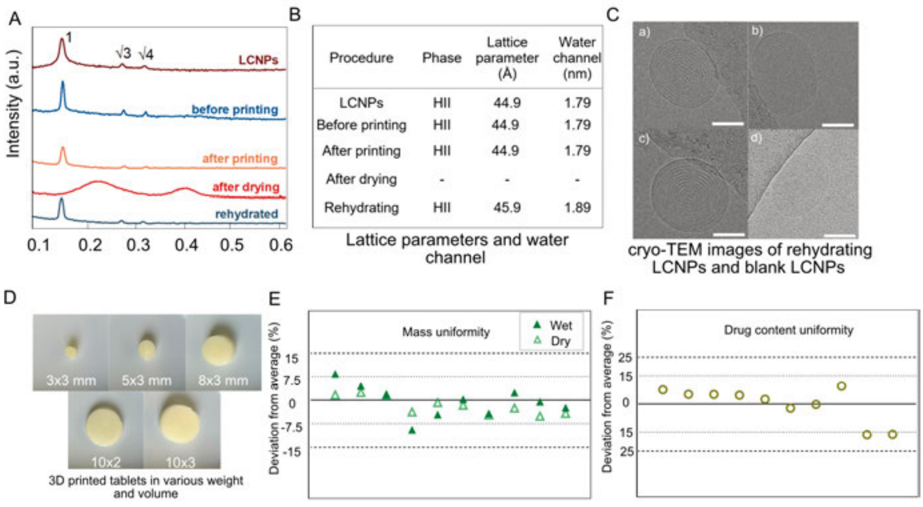

Figure 19. Structural confirmation of PHY/TOC LCNPs (in formulation 7) during gel preparation, 3D-printing and tablet rehydration and analysis of mass uniformity mass and dose accuracy across 3D-printed tablets based on lead formulation (**A**) Representative 1D SAXS patterns of intensity vs q of PHY/TOC LCNPs in different states: equilibrated LCNPs (dark red), gel before-printing (blue), 3D printed tablet (wet) (orange), and printed tablet after drying (orange) and after tablet rehydrating (dark blue). (**B**) Internal phase, lattice parameter and water channel of PHY/TOC LCNPs under different conditions. (**C**) Representative cryo-TEM image of rehydrating tablet (a, b, and c) and reference LCNPs (d). Scale bar = 100 nm. (**D**) Representative images of five 3D-printed tablets. (**E**) Uniformity of mass, represented as deviation from the average mass of individual tablets (n = 3). Wet weights (green triangles), dry weights (open green triangles). (**F**) Uniformity of drug content for the same batch of tablets (10x3 mm, n = 10), represented as deviation from the average VAN content. (n = 3).

These results highlight the robust structural integrity of PHY/TOC LCNPs throughout the tablet fabrication process. This demonstrates that combination drug dosage loaded inside of LCNPs can be monitored by modifying the mass, infill density, and pattern of the 3D-printed tablet within standard parameters. This is a significant benefit of SSE 3D printing, allowing for the manufacture of tablets that meet strict quality standards and enabling precise dose accuracy.

Conclusions

This thesis presents a comprehensive framework for developing LCNP-based oral antibiotic delivery systems that address the critical challenges of antimicrobial resistance through improved drug accessibility and bioavailability. The work integrates molecular-level understanding with pharmaceutical development and advanced manufacturing technologies to create next-generation nanomedicines. The systematic investigation spans from fundamental drug-LCNP interactions to proof of concept 3D printing production methods, establishing a translational pipeline for oral antibiotic formulations.

Specific conclusions of this thesis are:

- LCNPs based on enzymatically stable lipids (PHY/TOC and PHY/FAR) achieved >84% encapsulation efficiency for both hydrophilic (VAN) and hydrophobic (CLA) antibiotics, demonstrating versatility for combination therapy. (Paper I)
- The formulations exhibited exceptional enzymatic resistance (<2.6% lipolysis) in simulated intestinal fluids, ensuring structural integrity during gastrointestinal transit. (Paper I)
- Co-administered LCNPs provided significant protection to commensal bacteria, with MIC values exceeding detection limits (>1024 µg/mL) against *E. coli*, validating the strategy of targeted antibiotic delivery with minimal gut microbiota disruption. (Paper I)
- Drug localization was governed by physicochemical properties: clarithromycin accumulated in lipid domains (75% contact), while vancomycin equilibrated at water-lipid interfaces (50% each phase). (Paper II)
- Progressive polymer-water-lipid interface reorganization reduced release energy barriers 2-fold for clarithromycin and 3-fold for vancomycin. (Paper II)
- *In vitro* validation confirmed simulation predictions with 10% clarithromycin and 15% vancomycin burst release within 10 min, establishing structure-release relationships. (Paper II)

- Non-lamellar LCNPs achieved 95.6-99.1% cellular uptake versus 70.8% for conventional liposomes through energy-independent, curvature-driven mechanisms. (Paper III)
- Endocytosis inhibition studies revealed LCNPs maintained >90% uptake under dual endocytic inhibition, confirming non-endocytic internalization pathways. (Paper III)
- PHY cubosomes enhanced VAN permeability 13-fold ($P_{app} = 6.0 \times 10^{-5}$ cm/s) compared to free drug, with the ranking PHY > PHY/TOC > PHY/FAR > DOPC correlating with cellular uptake patterns. (Paper III)
- Optimized gel formulations (8.4% Ac-Di-Sol, 4.2% MC A4C, 3.6% MC A4M) enabled reproducible printing at 140-200 kPa pressure. (Paper IV)
- LCNPs spontaneously recovered hexagonal phase structure upon tablet rehydration without protective excipients, demonstrating intrinsic formulation stability. (Paper IV)
- Printed tablets met all Ph. Eur. requirements for mass uniformity (<7.5% deviation), and achieved predictable dose personalization ($R^2 = 0.93$ for drug content-weight correlation). (Paper IV)

Future perspectives

LCNPs have garnered significant interest due to their dual potential in therapeutic and diagnostic applications for oral antibiotic delivery. Owing to their unique internal nanostructures and biocompatibility, they represent a promising platform in the evolving field of nanomedicine. While this thesis has demonstrated the feasibility of LCNP-based oral formulations through systematic development from molecular to application, several challenges remain in translating these advancements to widespread clinical implementation.

The enzymatic stability of non-ester lipids used in LCNP formulation represents both a strength and a limitation. While PHY, TOC, and FAR resist pancreatic lipase degradation, ensuring cargo protection during GI transit, their metabolic fate and long-term biocompatibility require comprehensive investigation. Addressing this challenge necessitates systematic biodistribution studies, evaluating accumulation in reticuloendothelial organs, and establishing clearance mechanisms. The development of biodegradable alternatives that maintain structural integrity during transit while enabling controlled degradation post-absorption could enhance clinical acceptability.

The heterogeneous nature of internal mesophases presents another significant obstacle. While this thesis demonstrated successful H_{II} and Q_{II} phase formulations, achieving monodisperse populations with uniform internal structures remains challenging. Post-formulation processing steps such as size fractionation or density gradient centrifugation may be required, though these must remain scalable and complementary to the manufacturing process. In such cases, it is necessary to evaluate whether the enhanced performance justifies the increased complexity and cost compared to conventional liposomal formulations.

Molecular dynamics simulations revealed drug-specific compartmentalization within LCNPs, yet predicting this behavior for new therapeutic cargos remains empirical. Machine learning approaches could potentially identify hidden correlations between drug physicochemical properties, lipid composition, and compartmentalization patterns. Training models on expanded datasets encompassing diverse antibiotic classes, peptides, and combination therapies could enable rational design of tailored LCNP formulations. Such computational frameworks would accelerate formulation development while minimizing experimental iterations.

The mechanistic understanding of LCNP-epithelium interactions warrants further investigation at the tissue level. While Caco-2 monolayers provided valuable insights into permeation of lipid nanoparticles, more complex models incorporating mucus layers, M cells, and immune components would better predict *in vivo* performance. Additionally, the fate of LCNPs following transcellular transport, whether they remain intact or release cargo intracellularly, requires elucidation using advanced imaging techniques such as correlative light-electron microscopy or higher-resolution fluorescence microscopy.

SSE 3D printing demonstrated remarkable potential for personalized dosing, yet several manufacturing challenges require resolution. The heterogeneous distribution of LCNPs within printed tablets could lead to content uniformity issues at larger scales. Implementing in-line quality control measures such as near-infrared spectroscopy or Raman mapping could ensure consistent drug distribution. Furthermore, establishing regulatory frameworks for point-of-care 3D printing remains critical. Unlike conventional manufacturing, personalized production requires new quality assurance paradigms balancing flexibility with pharmaceutical standards.

The protective effect on gut microbiota, while promising, was evaluated using only two bacterial strains. Comprehensive microbiome studies employing rRNA sequencing or shotgun metagenomics would reveal broader ecological impacts. Understanding how LCNPs interact with the complex microbial consortium, including effects on bacterial metabolites and host-microbe interactions, is essential for predicting clinical outcomes. Furthermore, investigating whether certain bacterial species preferentially uptake LCNPs could explain the differential protection observed between Gram-positive and Gram-negative bacteria.

Translation to *in vivo* models presents both opportunities and challenges. Pharmacokinetic studies in relevant infection models would establish whether the enhanced permeability observed in vitro translates to therapeutic plasma concentrations. Key parameters requiring evaluation include oral bioavailability, tissue distribution, and the relationship between LCNP dose and systemic exposure. Additionally, assessing efficacy against resistant bacterial strains in systemic infection models would validate the clinical potential of this approach.

The combination therapy strategy demonstrated in this thesis could be expanded to address specific resistance mechanisms. Incorporating β-lactamase inhibitors, efflux pump inhibitors, or membrane-permeabilizing peptides within LCNPs could restore sensitivity to conventional antibiotics. The compartmentalized structure of LCNPs enables spatial separation of incompatible drugs, potentially enabling novel combination strategies previously limited by chemical instability or antagonistic interactions.

Finally, the manufacturing scalability demonstrated through pilot-scale production and 3D printing integration positions LCNP technology for clinical translation. However, cost-effectiveness analyses comparing LCNP formulations to conventional therapies remain essential. Factors including reduced dosing frequency, decreased resistance development, and improved patient compliance must be quantified to justify the increased complexity. Establishing partnerships with pharmaceutical companies and regulatory agencies early in development would facilitate the transition from academic innovation to clinical reality.

Acknowledgements

This PhD journey would not have been possible without the support, guidance, and encouragement of many individuals who shaped both my research and personal growth over these years.

The work presented in this thesis was conducted at the Department of Pharmacy, Uppsala University, with generous financial support from Uppsala Antibiotic Center and Swedeliver. I am particularly grateful to Apotekarsocieteten and CSC () for additional funding that enabled my participation in essential courses and conferences.

Supervisors

My deepest gratitude goes to my main supervisor, **Madlen Hubert**, for believing in my ability to tackle this multidisciplinary project from the very beginning. Your structured guidance through the complexities of different experimental approaches, your patience with my endless questions and mistakes, your unwavering support during presentations and manuscript preparations, and your pursuit of scientific rigor and attention to detail shaped me into an independent researcher. Thank you for encouraging ambitious ideas while keeping me grounded in scientific principles.

To my co-supervisor, **Christel Bergström**, your contribution to my academic development has been invaluable. Thank you for being the main supervisor for the first two years. Your ability to pinpoint the most critical aspects of any problem with almost instinctive precision, your expertise in making tough decisions and judgments. Thank you for always making time for insightful discussions that pushed my research and motivation forward. Your strategic vision and decisive leadership created an environment where innovative research could flourish.

I am thankful to all the students I have supervised. Supervising you taught me patience, clarity in communication, and the joy of watching young scientists grow. Together, growing with you, I have learned so much.

Here are all the names sorted alphabetically with their associated content:

Agnes - thank you for supporting me like an academic mother during the most confusing first two year of my PhD. Thank you for making me feel stronger and more resilient on this journey. I am deeply grateful to have met you and gotten to know you. Thank you for countless protocols, for teaching me hand-by-hand how to understand physical chemistry formulas, for innumerable words of comfort and encouragement, and for believing in me unwaveringly from beginning to end.

Alina - thank you for your kind and friendly support in the lab! Big congratulation for your defense! Dr. Meyer! Hope all the best for your next journey and have fun!

Aleksei - thank you for your assistance with MD simulation and for patiently explaining each analysis until I finally understood it. Your teaching made complex spectroscopic techniques accessible! Hope all the best for your new next step and also have fun!

Alexandra Teleki - thank you for your expertise. Your different kind of introverted, gentle yet determined strength showed me another dimension of female leadership.

Anano - thank you for your support throughout this journey. Your mental support and constant hugs meant a great deal. All the best with your journey and I'm sure you will tackle it very smooth!

Benyamin - thank you for introducing me to computational modelling for the movement in GIT and for helping me understand the complexities of mechanisms. You really have impressive style of speaking! Keep shining and keep being creative!

Caroline – thank you for all the efforts of taking care of Swedeliver, our lab and us. Thank you for showing us that great scientist can also be great multitasker!

Clarris – Even you are just being here for 1 month, I still want to thank you for joining our team, and be my summer student! It is so much fun to solve problem with you, hope all the best for your next journey.

Daisy - you are a person with a golden heart, always thinking about how to help others. Your warmth and kindness have been inspiring and encouraging to me constantly, well…you have set such high standard I don't think I can manage to get there. Your serious dedication to research and enthusiasm, your mastery of every technique and instrument, made me realize just how much a person can learn. Thank you for showing me what a true scientist looks like, for always encouraging me and helping me overcome my laziness and burnout, and for always being there.

Diyar - you made MD simulation seem so interesting. Your presentation was impressive, and your troubleshooting skills inspired me a lot (Especially when I re-read the MD simulation-umbrella sampling part…). Thank you for your efforts and thank you for the fika! We should have more!

Ellen - thank you for your help with FDR. Thank you for being so professional, efficient and FUN! I enjoy every time talking with you and check how is going with you, hope allll the best for your defense!

Eva - you are such a rich and colorful person. Thank you for letting me understand other sides of you, for your support of me at UAC, for your listening and understanding, for your comfort and encouragement. Every time I met you in the corridor, I felt reassured to be cared for by someone like you at UAC.

Evgenia - thank you for your LCMS expertise! You are the true master in it, and everyone knows it. Thank you for heling me to fix error until 20:00…You are also so strong! Hope all your next journey goes smooth and most importantly, have fun!

Edgar – great to have ML experts in the lab! I am very happy to have you in the group and I hope all the best for your PhD journey and have fun (most important)!

Foteini - your dedication to your master thesis taught me as much as I taught you. Thank you for being like a little sunshine in the lab, and always being so helpful, wishing your PhD journal goes well!

Hannah - thank you for your support and encouragement. Thank you for all the discussion with lipolysis, with permeability assay, and thank you for being so open-hearted to me. Your presence in the department was always uplifting!

Hanna - thank you for your support and encouragement! Your rehearsal discussion is so cute, and I will miss you a lot! Wishing your PhD journal goes well!

Helen - thank you for your help with the bacteria, thank you for showing me how to make the plate and stop me add more experiments on the first paper, you are so wise! I also had a lot fun when I get to know you more, and I think you are always our model.

Ilse - thank you for your support and I really enjoy the whole time throughout my master, the summer and some fika time. It is so happy to see you sometimes in the corridor, time really flies, I hope all your research, life and everything went smoothly.

Ivailo - Thank you, Caco-man! Thank you for seriously teaching me permeability studies countless times, for always telling me the details and sharing your experience, for giving me innumerable Caco-2 cells! Without these, I could not have graduated. Sometimes just seeing you in the cell culture room made me feel incredibly reassured, confident that these experiments would definitely work out.

Jiaxi - thank you for your support and friendship. After knowing you for so many years, I appreciate how you have always asked me when I was sick, always give me friends hug and always cared about me.

Johan Gråsjö - thank you for answering my SAXS questions every time I got stuck, even after five o'clock. You were always patient in telling me not to rush, that it would be okay. Thank you for encouraging and comforting me each time I made mistakes, for always being there, for your tolerance, and for sharing theoretical formulas about polymer-LCNP interactions. Your support gave me confidence to persist through difficulties.

Johan Engblom - thank you for your encouragement, for inviting me to attend top-tier conferences in the field, for trusting me with your supportive gaze, and for gently yet sharply pointing out shortcomings and areas for improvement while giving very practical and sincere suggestions. I am very happy to have met you and learned from your feedback!

Joram Kuropka – I have so many words to say to you, so much appreciation, proud and best wishes to you. You are so talent! I really enjoy every time you ask me questions or find some bug in my papers or just discuss some challenging definition. I think you should keep following your curiosity and keep learning, I am sure you will do a fantastic job in whatever you feel for it. But importantly, take good care my friend! Wishing you all the best for your future!

Johanna Laru - thank you my mentor! Thank you for all the meeting, all the tips of handling work-life balance and dealing with obstacles. You are so wise and intelligent, wish I could be like you someday. Such a role model! I really appreciate all the wonderful energy and insightful, practical suggestions you gave me, wishing all the best for you and your family!

Krisztina - thank you for always appearing in the lab so gently. Your calm presence brought warmth to the research environment.

Lindon - thank you for your guidance on chemical structure questions. I still remember the first meeting with you. Your insights into molecular design informed our formulation strategies the first time.

Linus - thank you for your advices and supports throughout my PhD journey in UAC and IMBIM corridor, I really appreciate your input in my halftime, that clears a lot of my puzzle about antibiotics. I still remember the first time in UAC, you bring it up with my project and I feel so happy and proud of it.

Lingxiao – thank you for discussing with me about lipolysis, and being always very friendly with me, thank you for all the details gossip and fun stuff (sky diving)! I hope all the best for your PhD! And I am sure you will be a great job! Hope to see you in Chengdu!

Lidia – thank you for always taking care of everyone (and ofc me!). You are such a special one in the lab, always motivated by your energy and passion! Thank you so much for your expertise on 3D printing, I really enjoy working with you and also learned a lot from you. I hope allll the best for your PhD! And I am 100% sure you will do a super great job! All the best my friend!

Maomin - thank you for helping me with so many Caco-2 cells. Having same office together with you was quite interesting too! Thank you for continuing to help me with all the trivial things. I hope you will take good care of yourself and I really appreciate your stand up more for yourself! Keep doing it!

Marco – thank you for your expertise on mucus! It was crucial for my puzzle with permeation problem. You are so extensively knowledgeable and helpful, my friend, I think you are such a nice person, wishing you all the best luck for your future and let's keep in touch!

Maria Karlgren - your course was one of my favorites during my master's studies. Thank you for continuously being tolerant of me—tolerating my impatience, my awkwardness and clumsiness. Thank you for your patience and smile; every time I saw your smile, I felt cared for.

Malhar - thank you for being so responsible and helpful in the lab. I am very glad that we have you such a great lab manager around us. Thank you so much for all the quite help, we all see them, and I wish all the best for you my friend and best of luck with all the next battles ahead!

Merve - thank you for your sense of humor and for bringing laughter to the lab. Your funny personality made challenging days lighter.

Mingjun - thank you for creating such a responsible atmosphere in the lab (especially with HPLC). I really appreciate your help with very detail and patient information every time I ask you. Wishing you all the best for your PhD and I am sure you will do a great job!

Paarkavi – thank you always for your kind smile and friendly hugs my friend. Thank you for supportive conversations during conference preparation. Your steadiness helped me through anxious moments.

Pacho - thank you for your guidance with flow cytometry techniques. Thank you for all the tips to handle data and life (PhD life especially). I am so grateful to have you help me with my last paper, and I wish all the best for you and your family!

Patrick - your post-doctoral wisdom about navigating academia was invaluable. Thank you for the career advice, for your expertise with LCMS, and for showing me that there's life after PhD. Your perspective helped me see beyond the immediate challenges.

Patrik Lundquist - thank you for your expertise and assistance with LCMS measurements. Your technical knowledge was essential for analytical work.

Prosper – thank you Prosper! You are always very curious and friendly with my project and me. It is very encouraging to see your projects goes so well too! Hope all the best with your PhD my friend!

Patricia Müller – I am so + very lucky to supervise you, thank you so much for your efforts and dedications on the projects. You are so sweet and clever, also very detail and curios. I still miss the time we were discussing on the white board! I wish you all the best for your future and I am sure you will do a wonderful job!

Per Hansson - thank you for the surfactants course, which was instrumental in strengthening my physical chemistry foundation. Thank you for your help with SAXS analysis, for your patience and smile, and for your consistent encouragement. Your teaching style made complex concepts more accessible and I am gonna miss the surfactants course (haha)

Philip - thank you for conducting MIC measurements and for sharing your expertise in antimicrobial testing. Your contributions were vital to demonstrating the therapeutic potential of our formulations. Thank you for spending few months to discuss with me, I have learn so many techniques with you.

Per L – your course is one of our favorite courses when I was doing my master. I can always reach out to you (our coordinator). Thank you for always being there for students, for taking care of us and clear the clouds above our head, and most importantly, for being so gentle and responsible for us.

Rekkah - thank you for your support, for the all the sweet cards, for your lovely words, for cute photos, and for your lovely energy. Your thoughtfulness and encouragement lifted my spirits during difficult times. I hope you will have a great time in PhD, and please take very good care of yourself, and don't be too strict to yourself.

Ruisheng - thank you for your assistance with NMR experiments. Your expertise in spectroscopic analysis enhanced the quality of our characterization work, thank you for your patience for explaining again and again with the software, I really enjoy working with you!

Shakhawath Hossain - thank you for introducing me to the world of MD when I first joined the group, while having my master program. Your expertise was invaluable, not just to me, but to everyone in the group (see how many collaborations you have). Your guidance in understanding structural parameter calculations also helped me a lot! Thank you!!!

Shahina - thank you for hugging me when the SAXS (or whatever) doesn’t work. When I see you, I feel mentally so much better! Thank you for being so friendly and kind to me, and always support me, I hope your PhD goes smooth! And I am sure you will nail it very well my friend!

Jason Qu - thank you for accompanying me while I was stressful and desperate, and for always doing your utmost to support me. Thank you for helping me fill out forms item by item, and for being so earnest even when you didn't fully understand. I am grateful to have met you. I am grateful for all the time you have spent with me. Thank you for always believing in me firmly, for always caring for me thoughtfully, and for allowing me to learn and grow.

Jonas – thank you for asking me questions and discuss with me about your project! So interesting! Wishing you all the best for your next journey and have a great time!

Yael - thank you for your passion and curiosity about research. I have always been inspired by you, and I hope we can go rock climbing together again in the future.

Yuming - thank you for your optimism. You are so fun to hangout, I wish we could have more time to hangout! Your positive attitude and made the lab atmosphere more enjoyable! All the best for your defense and I’m sure it will go super well!

I owe profound gratitude to my parents, my partner, and my best friend, whose unwavering support across geographical distance provided strength during challenging times. Despite being far away, you were always there when I needed you most.

Tingmo, so awesome to have you in this life, thank you for always being there, sometimes be disturbed by me even in the middle of the night. Thank you for immediately calling me when you noticed I was sad, lack of confidence or blue. I like your sensitiveness, your empathy and softness. Thank you bringing Afu to make me feel fulfilled and content inside. Thank you for taking care of me, for loving me, and for making me feel not alone, that I am not by myself.

Papa and Mama, thank you, both for your daily check-ins, for always trusting me and recognizing my efforts, for using your own achievements to inspire me, for consistently being proud of me, and for teaching me to be fearless and brave. Thank you also for loving me unconditionally, for inspiring me through your entrepreneurial spirit, and for faithfully sending me those exercise videos…even though I rarely click them, you never stop trying. Thank you both for creating such a warm, loving, and supportive family environment that gives me strength to face all of life's obstacles and challenges. I love you so much both.

Lastly, my wonderful partner **Philip**. Thank you for being so strong, so supportive, so kind and so patient whenever I was stressed from my career or life. And thank you for being so passionate about us, life and research! Your fire definitely encouraged me when I am down, blue and desperate. Thank you for making me to be the best versions of myself. Thank you for understanding my angry, anxiety, and fear deep in my soul and my inner child. Thank you for seeing me, hearing me, and loving me. Thank you for accepting who I really am, even the parts I do not want to accept myself. I have learned so much in the process of being with you. I am so grateful to have you in my life. I really feel excited for everyday with you.

To my friends in Uppsala: thank you for dinners, fikas, and mental supports that provided me essential entertainments. You made Uppsala feel like home.

Finally, to all unnamed individuals who contributed through corridor conversations, conference discussions, and collaborative meetings! Your collective wisdom shaped this thesis in countless ways.

Reference

1. Roope, L. S. J. *et al.* The challenge of antimicrobial resistance: What economics can contribute. *Science* **364**, eaau4679 (2019).
2. Nobel Prize in Physiology or Medicine 1945. *NobelPrize.org* https://www.nobelprize.org/prizes/medicine/1945/fleming/lecture/.
3. Antimicrobial resistance: tackling a crisis for the health and wealth of nations / the Review on Antimicrobial Resistance chaired by Jim O'Neill. *Wellcome Collection* https://wellcomecollection.org/works/rdpck35v.
4. Murray, C. J. *et al.* Global burden of bacterial antimicrobial resistance in 2019: a systematic analysis. *The Lancet* **0**, (2022).
5. MacGregor, R. R. & Graziani, A. L. Oral administration of antibiotics: a rational alternative to the parenteral route. *Clin. Infect. Dis. Off. Publ. Infect. Dis. Soc. Am.* **24**, 457–467 (1997).
6. Feeney, O. M. *et al.* 50years of oral lipid-based formulations: Provenance, progress and future perspectives. *Adv. Drug Deliv. Rev.* **101**, 167–194 (2016).
7. Hernando-Amado, S., Coque, T. M., Baquero, F. & Martínez, J. L. Defining and combating antibiotic resistance from One Health and Global Health perspectives. *Nat. Microbiol.* **4**, 1432–1442 (2019).
8. U.S. FDA. Drug Approval Package: AmBisome (Amphotericin B). Accessed 2025-08-08. https://www.accessdata.fda.gov/
9. ABELCET® (Amphotericin B Lipid Complex Injection) 100 mg. Label. Accessed 2025-08-08. https://nctr-crs.fda.gov/
10. Lipid-Based Nanoparticles for Drug/Gene Delivery: An Overview of the Production Techniques and Difficulties Encountered in Their Industrial Development - PubMed. https://pubmed.ncbi.nlm.nih.gov/38089666/.
11. Zhai, J., Fong, C., Tran, N. & Drummond, C. J. Non-Lamellar Lyotropic Liquid Crystalline Lipid Nanoparticles for the Next Generation of Nanomedicine. *ACS Nano* **13**, 6178–6206 (2019).
12. Barriga, H. M. G., Holme, M. N. & Stevens, M. M. Cubosomes: The Next Generation of Smart Lipid Nanoparticles? *Angew. Chem. Int. Ed.* **58**, 2958–2978 (2019).
13. Wye-Khay Fong, Renata Negrini, Jijo J. Vallooran, Raffaele Mezzenga, & Ben J. Boyd. Responsive self-assembled nanostructured lipid systems for drug delivery and diagnostics. *J. Colloid Interface Sci.* **484**, 320–339 (2016).
14. Bisoyi, H. K. & Li, Q. Liquid Crystals: Versatile Self-Organized Smart Soft Materials. *Chem. Rev.* **122**, 4887–4926 (2022).
15. Israelachvili, J. N., Mitchell, D. J. & Ninham, B. W. Theory of self-assembly of lipid bilayers and vesicles. *Biochim. Biophys. Acta* **470**, 185–201 (1977).
16. Shan, X., Luo, L., Yu, Z. & You, J. Recent advances in versatile inverse lyotropic liquid crystals. *J. Controlled Release* **348**, 1–21 (2022).
17. Celesta Fong, Tu C. Le, & Calum J. Drummond. Lyotropic liquid crystal engineering–ordered nanostructured small molecule amphiphile self-assembly materials by design. *Chem. Soc. Rev.* **41**, 1297–1322 (2012).

18. Van ‘T Hag, L., Gras, S. L., Conn, C. E. & Drummond, C. J. Lyotropic liquid crystal engineering moving beyond binary compositional space – ordered nanostructured amphiphile self-assembly materials by design. *Chem. Soc. Rev.* **46**, 2705–2731 (2017).
19. Anan Yaghmur, Anan Yaghmur, Huiling Mu, & Huiling Mu. Recent advances in drug delivery applications of cubosomes, hexosomes, and solid lipid nanoparticles. *Acta Pharm. Sin. B* **11**, 871–885 (2021).
20. Singh, S., Kushwah, V., Agrawal, A. K. & Jain, S. Insulin- and quercetin-loaded liquid crystalline nanoparticles: implications on oral bioavailability, antidiabetic and antioxidant efficacy. *Nanomed.* **13**, 521–537 (2018).
21. Agrawal, A. K., Kumar, K., Swarnakar, N. K., Kushwah, V. & Jain, S. “Liquid Crystalline Nanoparticles”: Rationally Designed Vehicle To Improve Stability and Therapeutic Efficacy of Insulin Following Oral Administration. *Mol. Pharm.* **14**, 1874–1882 (2017).
22. He, X. *et al.* Liquid crystal nanoparticles for oral combination antibiotic therapies: A strategy towards protecting commensal gut bacteria during treatment. *J. Colloid Interface Sci.* **678**, 287–300 (2025).
23. Borgheti-Cardoso, L. N. *et al.* An *in situ* gelling liquid crystalline system based on monoglycerides and polyethylenimine for local delivery of siRNAs. *Eur. J. Pharm. Sci.* **74**, 103–117 (2015).
24. Badea, I., Wettig, S., Verrall, R. & Foldvari, M. Topical non-invasive gene delivery using gemini nanoparticles in interferon-gamma-deficient mice. *Eur. J. Pharm. Biopharm. Off. J. Arbeitsgemeinschaft Pharm. Verfahrenstechnik EV* **65**, 414–422 (2007).
25. Rodrigues, L. *et al.* Immune responses induced by nano-self-assembled lipid adjuvants based on a monomycoloyl glycerol analogue after vaccination with the Chlamydia trachomatis major outer membrane protein. *J. Control. Release Off. J. Control. Release Soc.* **285**, 12–22 (2018).
26. Rizwan, S. B., Hanley, T., Boyd, B. J., Rades, T. & Hook, S. Liquid Crystalline Systems of Phytantriol and Glyceryl Monooleate Containing a Hydrophilic Protein: Characterisation, Swelling and Release Kinetics. *J. Pharm. Sci.* **98**, 4191–4204 (2009).
27. Evenbratt, H., Jonsson, C., Faergemann, J., Engström, S. & Ericson, M. B. In vivo study of an instantly formed lipid-water cubic phase formulation for efficient topical delivery of aminolevulinic acid and methyl-aminolevulinate. *Int. J. Pharm.* **452**, 270–275 (2013).
28. Morin, M., Björklund, S., Nilsson, E. J. & Engblom, J. Bicontinuous Cubic Liquid Crystals as Potential Matrices for Non-Invasive Topical Sampling of Low-Molecular-Weight Biomarkers. *Pharmaceutics* **15**, 2031 (2023).
29. Algarni, A. *et al. In vivo* delivery of plasmid DNA by lipid nanoparticles: the influence of ionizable cationic lipids on organ-selective gene expression. *Biomater. Sci.* **10**, 2940–2952 (2022).
30. Couvreur, P. *et al.* Discovery of new hexagonal supramolecular nanostructures formed by squalenoylation of an anticancer nucleoside analogue. *Small Weinh. Bergstr. Ger.* **4**, 247–253 (2008).
31. Johnsson, M., Barauskas, J., Norlin, A. & Tiberg, F. Physicochemical and Drug Delivery Aspects of Lipid-Based Liquid Crystalline Nanoparticles: A Case Study of Intravenously Administered Propofol. *J. Nanosci. Nanotechnol.* **6**, 3017–3024 (2006).
32. Cervin, C. *et al.* Properties and effects of a novel liquid crystal nanoparticle formulation of docetaxel in a prostate cancer mouse model. *Eur. J. Pharm. Sci. Off. J. Eur. Fed. Pharm. Sci.* **41**, 369–375 (2010).

33. Bryant, S. J., Bathke, E. K. & Edler, K. J. Bottom-up cubosome synthesis without organic solvents. *J. Colloid Interface Sci.* **601**, 98–105 (2021).
34. Gustafsson, J., LjusbergWahren, H., Almgren, M. & Larsson, K. Cubic lipid-water phase dispersed into submicron particles. *Langmuir* **12**, 4611–4613 (1996).
35. Gustafsson, J., Ljusberg-Wahren, H., Almgren, M. & Larsson, K. Submicron particles of reversed lipid phases in water stabilized by a nonionic amphiphilic polymer. *LANGMUIR* **13**, 6964–6971 (1997).
36. Spicer, P. T., Hayden, K. L., Lynch, M. L., Ofori-Boateng, A. & Burns, J. L. Novel Process for Producing Cubic Liquid Crystalline Nanoparticles (Cubosomes). *Langmuir* **17**, 5748 (2001).
37. Yu, H. *et al.* Formation of particulate lipid lyotropic liquid crystalline nanocarriers using a microfluidic platform. *J. Colloid Interface Sci.* **634**, 279–289 (2023).
38. Deng, J., Han, D. & Yang, J. Applications of Microfluidics in Liquid Crystal-Based Biosensors. *Biosensors* **11**, 385 (2021).
39. Dong, Y.-D., Larson, I., Hanley, T. & Boyd, B. J. Bulk and dispersed aqueous phase behavior of phytantriol: effect of vitamin E acetate and F127 polymer on liquid crystal nanostructure. *Langmuir ACS J. Surf. Colloids* **22**, 9512–9518 (2006).
40. Marco Fornasier *et al.* Cubosomes stabilized by a polyphosphoester-analog of Pluronic F127 with reduced cytotoxicity. *J. Colloid Interface Sci.* **580**, 286–297 (2020).
41. Barauskas, J. & Landh, T. Phase behavior of the phytantriol/water system. *Langmuir* **19**, 9562–9565 (2003).
42. Boyd, B. J., Whittaker, D. V., Khoo, S.-M. & Davey, G. Lyotropic liquid crystalline phases formed from glycerate surfactants as sustained release drug delivery systems. *Int. J. Pharm.* **309**, 218–226 (2006).
43. Nguyen, T.-H., Hanley, T., Porter, C. J. H. & Boyd, B. J. Nanostructured reverse hexagonal liquid crystals sustain plasma concentrations for a poorly water-soluble drug after oral administration. *Drug Deliv. Transl. Res.* **1**, 429–438 (2011).
44. Diaa Abdullah, H., Kamal, I., Sabry, S. A., Abd elghany, M. & El hakim Ramadan, A. Clarithromycin-tailored cubosome: A sustained release oral nano platform for evaluating antibacterial, anti-biofilm, anti-inflammatory, anti-liver cancer, biocompatibility, ex-vivo and in-vivo studies. *Int. J. Pharm.* **667**, 124865 (2024).
45. Nithya, R., Jerold, P. & Siram, K. Cubosomes of dapsone enhanced permeation across the skin. *J. Drug Deliv. Sci. Technol.* **48**, 75–81 (2018).
46. Alharbi, W. S. & Hosny, K. M. Development and optimization of ocular *in situ* gels loaded with ciprofloxacin cubic liquid crystalline nanoparticles. *J. Drug Deliv. Sci. Technol.* **57**, 101710 (2020).
47. Gitte, M., Sudhakar Gomte, S., Girish Agnihotri, T., Singh, N. & Jain, A. Development of amoxicillin Trihydrate-Loaded lyotropic liquid crystal nanoparticles for skin infection. *J. Mol. Liq.* **374**, 121281 (2023).
48. Awad, M., Barnes, T. J., Thomas, N., Joyce, P. & Prestidge, C. A. Gallium Protoporphyrin Liquid Crystalline Lipid Nanoparticles: A Third-Generation Photosensitizer against Pseudomonas aeruginosa Biofilms. *Pharmaceutics* **14**, 2124 (2022).

49. Kaul, S., Nagaich, U. & Verma, N. Investigating nanostructured liquid crystalline particles as prospective ocular delivery vehicle for tobramycin sulfate: Ex vivo and in vivo studies. *J. Adv. Pharm. Technol. Res.* **12**, 356–361 (2021).
50. Thorn, C. R. *et al.* Liquid crystal nanoparticle platform for increased efficacy of cationic antimicrobials against biofilm infections. *Nanomedicine Nanotechnol. Biol. Med.* **42**, 102536 (2022).
51. Awad, M., Barnes, T. J., Joyce, P., Thomas, N. & Prestidge, C. A. Liquid crystalline lipid nanoparticle promotes the photodynamic activity of gallium protoporphyrin against S. aureus biofilms. *J. Photochem. Photobiol. B* **232**, 112474 (2022).
52. Liu, R. *et al.* Liquid Crystalline Nanoparticles as an Ophthalmic Delivery System for Tetrandrine: Development, Characterization, and In Vitro and In Vivo Evaluation. *Nanoscale Res. Lett.* **11**, 254 (2016).
53. Awad, M., Barnes, T. J. & Prestidge, C. A. Lyophilized Lipid Liquid Crystalline Nanoparticles as an Antimicrobial Delivery System. *Antibiotics* **12**, 1405 (2023).
54. Kim, M. *et al.* Novel piperazine-based ionizable lipid nanoparticles allow the repeated dose of mRNA to fibrotic lungs with improved potency and safety. *Bioeng. Transl. Med.* **8**, e10556 (2023).
55. Ramirez, G. *et al.* Sustained absorption of delamanid from lipid-based formulations as a path to reduced frequency of administration. *Drug Deliv. Transl. Res.* **11**, 1236–1244 (2021).
56. Zheng, J., Zhang, Y. & Zhang, S. Sustained release of azithromycin from lipid liquid-crystalline nanoparticles laden in situ gel for the treatment of periodontitis: In vitro and efficacy study. *J. Biomater. Appl.* **37**, 482–492 (2022).
57. Khan, S. *et al.* Topical Delivery of Erythromycin Through Cubosomes for Acne. *Pharm. Nanotechnol.* **6**, 38–47 (2018).
58. Ahsan, A., Barnes, T. J., Thomas, N., Subramaniam, S. & Prestidge, C. A. Lipid-based nanocarriers for enhanced gentamicin delivery: a comparative study of liquid crystal nanoparticles and liposomes against Escherichia coli biofilms. *Drug Deliv. Transl. Res.* https://doi.org/10.1007/s13346-025-01890-0 (2025) doi:10.1007/s13346-025-01890-0.
59. Ramalheiro, A., Paris, J. L., Silva, B. F. B. & Pires, L. R. Rapidly dissolving microneedles for the delivery of cubosome-like liquid crystalline nanoparticles with sustained release of rapamycin. *Int. J. Pharm.* **591**, 119942 (2020).
60. Håkansson, J. *et al.* Characterization of the in vitro, ex vivo, and in vivo Efficacy of the Antimicrobial Peptide DPK-060 Used for Topical Treatment. *Front. Cell. Infect. Microbiol.* **9**, 174 (2019).
61. Valentin, J. D. P., Kadakia, P., Varidel, L. J., Stuart, M. C. A. & Salentinig, S. Colloidal Structure Dictates Antimicrobial Efficacy in LL-37 Self-Assemblies With Glycerol Monooleate. *Small* **20**, 2405131 (2024).
62. Boge, L. *et al.* Cubosomes for topical delivery of the antimicrobial peptide LL-37. *Eur. J. Pharm. Biopharm. Off. J. Arbeitsgemeinschaft Pharm. Verfahrenstechnik EV* **134**, 60–67 (2019).
63. Boge, L. *et al.* Cubosomes post-loaded with antimicrobial peptides: characterization, bactericidal effect and proteolytic stability. *Int. J. Pharm.* **526**, 400–412 (2017).
64. Boge, L. *et al.* Lipid-Based Liquid Crystals As Carriers for Antimicrobial Peptides: Phase Behavior and Antimicrobial Effect. *Langmuir ACS J. Surf. Colloids* **32**, 4217–4228 (2016).

65. Thorn, C. R. *et al.* Liquid crystal nanoparticle platform for increased efficacy of cationic antimicrobials against biofilm infections. *Nanomedicine Nanotechnol. Biol. Med.* **42**, 102536 (2022).
66. Subramaniam, S., Joyce, P. & Prestidge, C. A. Liquid crystalline lipid nanoparticles improve the antibacterial activity of tobramycin and vancomycin against intracellular Pseudomonas aeruginosa and Staphylococcus aureus. *Int. J. Pharm.* **639**, 122927 (2023).
67. Martin-Serrano, Á., Gómez, R., Ortega, P. & de la Mata, F. J. Nanosystems as Vehicles for the Delivery of Antimicrobial Peptides (AMPs). *Pharmaceutics* **11**, 448 (2019).
68. Milak, S., Chemelli, A., Glatter, O. & Zimmer, A. Vancomycin ocular delivery systems based on glycerol monooleate reversed hexagonal and reversed cubic liquid crystalline phases. *Eur. J. Pharm. Biopharm. Off. J. Arbeitsgemeinschaft Pharm. Verfahrenstechnik EV* **139**, 279–290 (2019).
69. Chen, Y.-H. *et al.* Vancomycin-Loaded Nanoparticles Enhance Sporicidal and Antibacterial Efficacy for Clostridium difficile Infection. *Front. Microbiol.* **10**, (2019).
70. Iudin, D. *et al.* Polypeptide Self-Assembled Nanoparticles as Delivery Systems for Polymyxins B and E. *Pharmaceutics* **12**, 868 (2020).
71. Tran, N. *et al.* Non-lamellar lyotropic liquid crystalline nanoparticles enhance the antibacterial effects of rifampicin against *Staphylococcus aureus*. *J. Colloid Interface Sci.* **519**, 107–118 (2018).
72. Boyd, B. J. & Boyd, B. J. Characterisation of drug release from cubosomes using the pressure ultrafiltration method. *Int. J. Pharm.* **260**, 239–247 (2003).
73. Wolska, E. & Szymańska, M. Comparison of the In Vitro Drug Release Methods for the Selection of Test Conditions to Characterize Solid Lipid Microparticles. *Pharmaceutics* **15**, 511 (2023).
74. Dawoud, M. Z. & Nasr, M. Comparison of drug release from liquid crystalline monoolein dispersions and solid lipid nanoparticles using a flow cytometric technique. *Acta Pharm. Sin. B* **6**, 163–169 (2016).
75. Boyd, B. J., Khoo, S.-M., Whittaker, D. V., Davey, G. & Porter, C. J. H. A lipid-based liquid crystalline matrix that provides sustained release and enhanced oral bioavailability for a model poorly water soluble drug in rats. *Int. J. Pharm.* **340**, 52–60 (2007).
76. Meikle, T. G. *et al.* Predicting the release profile of small molecules from within the ordered nanostructured lipidic bicontinuous cubic phase using translational diffusion coefficients determined by PFG-NMR. *Nanoscale* **9**, 2471–2478 (2017).
77. Negrini, R. & Mezzenga, R. Diffusion, Molecular Separation, and Drug Delivery from Lipid Mesophases with Tunable Water Channels. *Langmuir* **28**, 16455–16462 (2012).
78. Huang, Y. & Gui, S. Factors affecting the structure of lyotropic liquid crystals and the correlation between structure and drug diffusion. *RSC Adv.* **8**, 6978–6987 (2018).
79. Rennick, J. J., Johnston, A. P. R. & Parton, R. G. Key principles and methods for studying the endocytosis of biological and nanoparticle therapeutics. *Nat. Nanotechnol.* **16**, 266–276 (2021).
80. Rodrigues, L. *et al.* Cellular uptake of self-assembled phytantriol-based hexosomes is independent of major endocytic machineries. *J. Colloid Interface Sci.* **553**, 820–833 (2019).

81. Jagielski, J. *et al.* Comprehensive and comparative studies on nanocytotoxicity of glyceryl monooleate- and phytantriol-based lipid liquid crystalline nanoparticles. *J. Nanobiotechnology* **19**, 168 (2021).
82. Deshpande, S. & Singh, N. Influence of Cubosome Surface Architecture on Its Cellular Uptake Mechanism. *Langmuir ACS J. Surf. Colloids* **33**, 3509–3516 (2017).
83. Yap, S. L. *et al.* Cell interactions with lipid nanoparticles possessing different internal nanostructures: Liposomes, bicontinuous cubosomes, hexosomes, and discontinuous micellar cubosomes. *J. Colloid Interface Sci.* S002197972302177X (2023) doi:10.1016/j.jcis.2023.11.059.
84. Abdel-Bar, H. M. & El Basset Sanad, R. A. Endocytic pathways of optimized resveratrol cubosomes capturing into human hepatoma cells. *Biomed. Pharmacother. Biomedecine Pharmacother.* **93**, 561–569 (2017).
85. Yap, S. L. *et al.* The Internal Nanostructure of Lipid Nanoparticles Influences Their Diverse Cellular Uptake Pathways. *Small* **n/a**, 2500903.
86. Dyett, B. P., Yu, H., Strachan, J., Drummond, C. J. & Conn, C. E. Fusion dynamics of cubosome nanocarriers with model cell membranes. *Nat. Commun.* **10**, 4492 (2019).
87. Yap, S. L. *et al.* Bypassing Endocytic Barriers: Visualizing Membrane Fusion and Endosomal Escape of Cubic Phase Lipid Nanoparticles (Cubosomes). *Small* **n/a**, 2502231.
88. Yap, S. L. *et al.* Bypassing Endocytic Barriers: Visualizing Membrane Fusion and Endosomal Escape of Cubic Phase Lipid Nanoparticles (Cubosomes). *Small Weinh. Bergstr. Ger.* e2502231 (2025) doi:10.1002/smll.202502231.
89. Yap, S. L. *et al.* Cell interactions with lipid nanoparticles possessing different internal nanostructures: Liposomes, bicontinuous cubosomes, hexosomes, and discontinuous micellar cubosomes. *J. Colloid Interface Sci.* **656**, 409–423 (2024).
90. Nguyen, T.-H., Hanley, T., Porter, C. J. H. & Boyd, B. J. Nanostructured liquid crystalline particles provide long duration sustained-release effect for a poorly water soluble drug after oral administration. *J. Control. Release Off. J. Control. Release Soc.* **153**, 180–186 (2011).
91. Seoane-Viaño, I., Januskaite, P., Alvarez-Lorenzo, C., Basit, A. W. & Goyanes, A. Semi-solid extrusion 3D printing in drug delivery and biomedicine: Personalised solutions for healthcare challenges. *J. Control. Release Off. J. Control. Release Soc.* **332**, 367–389 (2021).
92. Trenfield, S. J., Awad, A., Goyanes, A., Gaisford, S. & Basit, A. W. 3D Printing Pharmaceuticals: Drug Development to Frontline Care. *Trends Pharmacol. Sci.* **39**, 440–451 (2018).
93. Pietrzak, K., Isreb, A. & Alhnan, M. A. A flexible-dose dispenser for immediate and extended release 3D printed tablets. *Eur. J. Pharm. Biopharm.* **96**, 380–387 (2015).
94. Khaled, S. A., Burley, J. C., Alexander, M. R., Yang, J. & Roberts, C. J. 3D printing of five-in-one dose combination polypill with defined immediate and sustained release profiles. *J. Control. Release Off. J. Control. Release Soc.* **217**, 308–314 (2015).
95. Breitkreutz, J. & Boos, J. Paediatric and geriatric drug delivery. *Expert Opin. Drug Deliv.* **4**, 37–45 (2007).
96. Subramaniam, S., Joyce, P. & Prestidge, C. A. Liquid crystalline lipid nanoparticles improve the antibacterial activity of tobramycin and vancomycin against intracellular *Pseudomonas aeruginosa* and *Staphylococcus aureus*. *Int. J. Pharm.* **639**, 122927 (2023).

97. Boge, L. *et al.* Lipid-Based Liquid Crystals As Carriers for Antimicrobial Peptides: Phase Behavior and Antimicrobial Effect. *Langmuir* **32**, 4217–4228 (2016).
98. Keemink, J., Mårtensson, E. & Bergström, C. A. S. Lipolysis-Permeation Setup for Simultaneous Study of Digestion and Absorption in Vitro. *Mol. Pharm.* **16**, 921–930 (2019).
99. Knight, C. J. & Hub, J. S. MemGen: a general web server for the setup of lipid membrane simulation systems. *Bioinforma. Oxf. Engl.* **31**, 2897–2899 (2015).
100. Boyd, K. J. & May, E. R. BUMPy: A Model-Independent Tool for Constructing Lipid Bilayers of Varying Curvature and Composition. *J. Chem. Theory Comput.* **14**, 6642–6652 (2018).
101. Martínez, L., Andrade, R., Birgin, E. G. & Martínez, J. M. PACKMOL: a package for building initial configurations for molecular dynamics simulations. *J. Comput. Chem.* **30**, 2157–2164 (2009).
102. Abraham, M. J. *et al.* GROMACS: High performance molecular simulations through multi-level parallelism from laptops to supercomputers. *SoftwareX* **1–2**, 19–25 (2015).
103. Huang, J. & MacKerell, A. D. CHARMM36 all-atom additive protein force field: validation based on comparison to NMR data. *J. Comput. Chem.* **34**, 2135–2145 (2013).
104. Vanommeslaeghe, K., Raman, E. P. & MacKerell, A. D. Automation of the CHARMM General Force Field (CGenFF) II: assignment of bonded parameters and partial atomic charges. *J. Chem. Inf. Model.* **52**, 3155–3168 (2012).
105. Vanommeslaeghe, K. & MacKerell, A. D. Automation of the CHARMM General Force Field (CGenFF) I: bond perception and atom typing. *J. Chem. Inf. Model.* **52**, 3144–3154 (2012).
106. Choi, Y. K. *et al.* CHARMM-GUI Polymer Builder for Modeling and Simulation of Synthetic Polymers. *J. Chem. Theory Comput.* **17**, 2431–2443 (2021).
107. Darden, T., York, D. & Pedersen, L. Particle mesh Ewald: An N·log(N) method for Ewald sums in large systems. *J. Chem. Phys.* **98**, 10089–10092 (1993).
108. Parrinello, M. & Rahman, A. Polymorphic transitions in single crystals: A new molecular dynamics method. *J. Appl. Phys.* **52**, 7182–7190 (1981).
109. Ramezanpour, M. *et al.* Structural Properties of Inverted Hexagonal Phase: A Hybrid Computational and Experimental Approach. *Langmuir ACS J. Surf. Colloids* **36**, 6668–6680 (2020).
110. Ramezanpour, M. & Tieleman, D. P. Computational Insights into the Role of Cholesterol in Inverted Hexagonal Phase Stabilization and Endosomal Drug Release. *Langmuir ACS J. Surf. Colloids* **38**, 7462–7471 (2022).
111. Hub, J. g_wham — A Free Weighted Histogram Analysis Implementation Including Robust Error and Autocorrelation Estimates. *Computational Biophysics Group* https://biophys.uni-saarland.de/publication/14-hub-jctc-2010/ (2010).
112. Artursson, P. & Karlsson, J. Correlation between oral drug absorption in humans and apparent drug permeability coefficients in human intestinal epithelial (Caco-2) cells. *Biochem. Biophys. Res. Commun.* **175**, 880–885 (1991).
113. Hubatsch, I., Ragnarsson, E. G. E. & Artursson, P. Determination of drug permeability and prediction of drug absorption in Caco-2 monolayers. *Nat. Protoc.* **2**, 2111–2119 (2007).

114. Macia, E. *et al.* Dynasore, a cell-permeable inhibitor of dynamin. *Dev. Cell* **10**, 839–850 (2006).
115. Chai, G.-H. *et al.* Transport Mechanisms of Solid Lipid Nanoparticles across Caco-2 Cell Monolayers and their Related Cytotoxicology. *ACS Appl. Mater. Interfaces* **8**, 5929–5940 (2016).
116. Johannesson, J., Khan, J., Hubert, M., Teleki, A. & Bergström, C. A. S. 3D-printing of solid lipid tablets from emulsion gels. *Int. J. Pharm.* **597**, 120304 (2021).
117. Johannesson, J., Wu, M., Johansson, M. & Bergström, C. A. S. Quality attributes for printable emulsion gels and 3D-printed tablets: Towards production of personalized dosage forms. *Int. J. Pharm.* **646**, 123413 (2023).
118. Hedge, O. J. & Bergström, C. A. S. Suitability of Artificial Membranes in Lipolysis-Permeation Assays of Oral Lipid-Based Formulations. *Pharm. Res.* **37**, 99 (2020).
119. Boehm, A. B. & Sassoubre, L. M. Enterococci as Indicators of Environmental Fecal Contamination. in *Enterococci: From Commensals to Leading Causes of Drug Resistant Infection* (eds Gilmore, M. S., Clewell, D. B., Ike, Y. & Shankar, N.) (Massachusetts Eye and Ear Infirmary, Boston, 2014).
120. Foster-Nyarko, E. & Pallen, M. J. The microbial ecology of Escherichia coli in the vertebrate gut. *FEMS Microbiol. Rev.* **46**, fuac008 (2022).
121. Mukherjee, D., Wu, M.-L., Teo, J. W. P. & Dick, T. Vancomycin and Clarithromycin Show Synergy against Mycobacterium abscessus In Vitro. *Antimicrob. Agents Chemother.* **61**, e01298-17 (2017).
122. Fujimura, S. *et al.* Combined efficacy of clarithromycin plus cefazolin or vancomycin against Staphylococcus aureus biofilms formed on titanium medical devices. *Int. J. Antimicrob. Agents* **32**, 481–484 (2008).
123. Kheyfets, B., Galimzyanov, T. & Mukhin, S. Lipid lateral self-diffusion drop at liquid-gel phase transition. *Phys. Rev. E* **99**, 012414 (2019).
124. Shendrik, P., Golani, G., Dharan, R., Schwarz, U. S. & Sorkin, R. Membrane Tension Inhibits Lipid Mixing by Increasing the Hemifusion Stalk Energy. *ACS Nano* **17**, 18942–18951 (2023).
125. Yap, S. L. *et al.* The Internal Nanostructure of Lipid Nanoparticles Influences Their Diverse Cellular Uptake Pathways. *Small Weinh. Bergstr. Ger.* e2500903 (2025) doi:10.1002/smll.202500903.
126. Rengaraj, R., Mariappan, S., Sekar, U. & Kamalanadhan, A. Detection of Vancomycin Resistance among Enterococcus faecalis and Staphylococcus aureus. *J. Clin. Diagn. Res. JCDR* **10**, DC04–DC06 (2016).
127. Akbari, A., Lavasanifar, A. & Wu, J. Interaction of cruciferin-based nanoparticles with Caco-2 cells and Caco-2/HT29-MTX co-cultures. *Acta Biomater.* **64**, 249–258 (2017).
128. Almeida, A. S., Silva, B., Remião, F. & Fernandes, C. Assessment of the Permeability of 3,4-Methylenedioxypyrovalerone (MDPV) across the Caco-2 Monolayer for Estimation of Intestinal Absorption and Enantioselectivity. *Int. J. Mol. Sci.* **24**, 2680 (2023).
129. Boge, L. *et al.* Freeze-dried and re-hydrated liquid crystalline nanoparticles stabilized with disaccharides for drug-delivery of the plectasin derivative AP114 antimicrobial peptide. *J. Colloid Interface Sci.* **522**, 126–135 (2018).

Acta Universitatis Upsaliensis

Digital Comprehensive Summaries of Uppsala Dissertations from the Faculty of Pharmacy 386

Editor: The Dean of the Faculty of Pharmacy

A doctoral dissertation from the Faculty of Pharmacy, Uppsala University, is usually a summary of a number of papers. A few copies of the complete dissertation are kept at major Swedish research libraries, while the summary alone is distributed internationally through the series Digital Comprehensive Summaries of Uppsala Dissertations from the Faculty of Pharmacy. (Prior to January, 2005, the series was published under the title "Comprehensive Summaries of Uppsala Dissertations from the Faculty of Pharmacy".)

ACTA UNIVERSITATIS
UPSALIENSIS
2025

Distribution: publications.uu.se
urn:nbn:se:uu:diva-568292